Wearable Electronics 1 (2024) 91–110

Contents lists available at ScienceDirect

Wearable Electronics

journal homepage: www.keaipublishing.com/en/journals/wearable-electronics

Review

Patterned growth of organic semiconductors for ultra-high resolution microelectronics and optoelectronics

Wenchong Wang[a,c], Lifeng Chi[b,d,*]

[a] Westfälische Wilhelms-Universität Münster, Physikalisches Institut and Center for Nanotechnology (CeNTech), Wilhelm-Klemm-Straße 10, Münster 48149, Germany
[b] Institute of Functional Nano & Soft Materials (FUNSOM), Jiangsu Key Laboratory for Carbon-Based Functional Materials & Devices, Soochow University, 199 Ren'ai Road, Suzhou, Jiangsu 215123, China
[c] Institution Center for Soft Nanoscience, Busso-Peus-Strasse10, Münster 48149, Germany
[d] Department of Materials Science and Engineering, Macau University of Science and Technology, Macau 999078, China

ARTICLE INFO

Keywords:
Organic semiconductors
Surface patterning
Patterned growth
Semiconductor devices

ABSTRACT

With intrinsic properties of flexibility, biocompatibility and lightweight, organic semiconductors have gained significant interests and witnessed substantial progresses in microelectronics and optoelectronics. Recently, the rapid development of wearable electronics such as near-eye displays requires the downscaling of the organic semiconductor devices to micrometers to provide immersive experiences and low power consumption. This review summarizes our work in patterned growth of organic semiconductors since 2007, with the aim of developing a photolithography compatible technology for ultra-high-resolution organic semiconductor devices. Upon deposition onto patterned surfaces, the organic molecules can be selectively grown on designated areas in three different mechanisms which are dependent on molecular chemical structure, deposition parameters, pre-pattern chemistry and dimensions. The three mechanisms, induced namely by binding energy difference, step-edges and surface molecular density modulation, can be rooted to initial nucleation of molecules, and analog to those in inorganic thin film growth at atomic scale. The patterned organic semiconductors can be engineered physically and dimensionally under various circumstances in vacuum, air, solution, or emulsion. Finally, employing these strategies, ultrahigh-resolution electronic and optoelectronic devices are demonstrated, and outlook of the further developments are discussed.

1. Introduction

1.1. Organic semiconductors and devices

Organic semiconductors are carbon-rich compounds that commonly possess an aromatic or conjugated π-electron system [1–5]. Remarkable advances in synthetic chemistry have enabled chemical modification of organic molecules by incorporating functional groups for designated electronic and optoelectronic properties [6–10]. For example, electron withdrawing and donating groups can be incorporated to facilitate the transport of p- and n-type carriers [11,12]. With advanced surface coating techniques, the p- and n-type materials can be successively deposited to form a p-n junction, laying the foundation for the building complex device structures [13–15].

In 1980 s, the appearance of thin film organic semiconductor devices provided great potential to revolutionize electronics [16–18]. Devices based on organic semiconductors are extensively explored, including organic field-effect transistors (OFETs) [19–21], organic light-emitting diodes (OLEDs) [22–25], organic solar cells (OSCs) [26,27], sensors [28,29] and more [30–32]. The organic semiconductor devices are typically constructed with active layers and electrodes. The active layers play crucial roles in carrier transporting, exciton recombination and separation according to their operation states [33]. In addition, the active layer are further fabricated on or connected to electrodes which can be addressed by external circuits [34]. Nowadays, the organic semiconductor devices have transitioned from conceptualization in laboratories to industrial products, particularly for the OLEDs that are extensively applied in portable and wearable devices such as mobile phones, smart watches, and near eye displays [35].

Peer review under the responsibility of Editorial Board of Wearable Electronics.
* Corresponding author at: Institute of Functional Nano & Soft Materials (FUNSOM), Jiangsu Key Laboratory for Carbon-Based Functional Materials & Devices, Soochow University, 199 Ren'ai Road, Suzhou, Jiangsu 215123, China.
E-mail address: chilf@suda.edu.cn (L. Chi).

https://doi.org/10.1016/j.wees.2024.05.005
Received 12 February 2024; Received in revised form 9 April 2024; Accepted 8 May 2024
Available online 15 May 2024

Recently, the wearable electronics are emerging novel platform for various applications in health monitoring, human-machine interface and entertainments [36,37]. Future developments of the wearable electronics strongly rely on material synthesis, functional films preparation, devices processing and monolithic integration. Among them, high resolution device pattering and processing, which could provide small device dimension and low operation voltage, play a vital role to achieve compact wearable systems with light weight, flexibility and low power consumption [38,39].

1.2. Growth dynamics of organic semiconductors by physical vapor deposition

Physical vapor deposition (PVD) is one of the mainstream thin film deposition techniques widely employed for small molecular organic semiconductors, using heating sources under a vacuum conditions [40]. The molecular beams that produced by the heating sources are deposited onto substrate surfaces, where the deposition rate is controlled by the source temperature. The vacuum circumstance is provided to keep the evaporated material from contamination, such as oxidation in air. In the meantime, the vacuum also ensure the vaporized molecular beams have a sufficient mean free path to reach the substrate surface. The technique provides a control accuracy of sub-molecular layer in thickness, which can be *in situ* monitored by quartz crystal microbalances. When absorbed onto substrate surface, the molecules can diffuse over the surface with their diffusivity controlled by substrate temperature [41]. With the PVD, multilayer deposition and co-deposition of several organic semiconductors are possible without the concerns of delamination or dissolution of the previous layers during subsequent deposition steps [42]. Although with relatively complicated equipment setups and high initial cost, the PVD has been successfully applied in small molecular organic semiconductor electronic devices, such as OLEDs, OFETs and OPVs, in both research and mass production.

Material growth from molecules by the PVD is a nonequilibrium process governed by the competition between kinetics and thermodynamics. The molecules, evaporated from the heating source, are directed to a relatively cold substrate surface. After absorbed onto the substrate surface, the molecules undergo diffusion, desorption, and nucleation on the surface [43]. The basic growth process of molecules, which involves nucleation at energetically favorable sites to form islands (aggregates) and their temporal evolution, is well characterized and found to closely mimic the epitaxial growth of inorganic materials [44]. In conventional nucleation theory, deposited molecules are thermally activated to diffuse on the surface to form islands (aggregates) by gathering several molecules together or nucleate at defect sites and step edges due to their relatively strong interaction to these specific locations, as schematically shown in Fig. 1. The nuclei, which are not stable

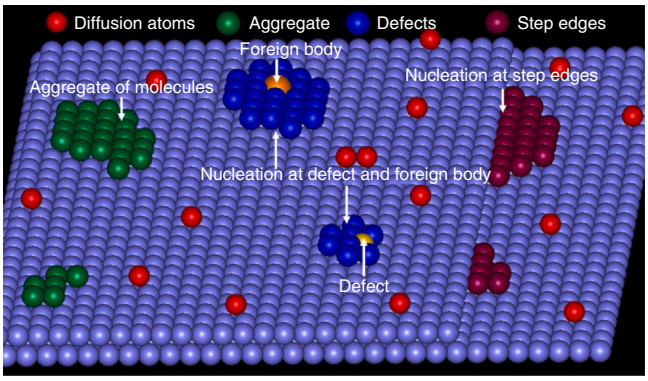

Fig. 1. Atomic-scale view of the molecule growth process at a surface. The deposited molecules can diffuse over the substrate surface to form aggregates by gathering molecules or nucleate at defects and step edges. The colored spheres represent molecules in the corresponding nucleation mechanisms.

in the initial stage when the size is smaller than a critical value, will either disappear via desorption or grow to form the stable ones by capturing further molecules [45].

1.3. Patterning strategies for organic semiconductors

The success of organic semiconductors will depend on patterning technology to produce high performance devices with scalability. Conventional device processing techniques based on photolithography and etching have been verified as powerful tools for inorganic semiconductors such as Si, GaAs and GaN [46]. Unfortunately, the techniques cannot be simply applied to pattern organic semiconductors owing to their fragile properties such as sensitivity to ultraviolet and oxidizing environments, as well as solubility in organic solvents [47]. A number of researchers have sought to develop photolithographic procedures by encapsulating organic materials into metal or photoresist layers [48], employing anisotropic photolithography with in-situ formed non-volatile etch barrier layer [49], and using direct photolithography with highly fluorinated materials and photo-crosslinking additives [50,51]. However, these photolithographic procedures still involve multi-step processing or are limited to specialized materials [52].

Alternative top-down strategies for organic semiconductor patterning are extensively explored, including fine metal mask (FMM), transfer printing and beam writing. The FMM patterning is an easily accessible technique that evaporated organics pass through small openings on a metal mask, forming patterns on a substrate [53]. With typical resolution ranging from 300 to 600 pixel per inches (ppi), the FMM technology dominates OLED displays fabrication for smartphones and notebook panels. Transfer printing refers to massive transfer of patterns with a physical master which could put on or take away organic materials/metals on sample surfaces [54,55]. The parallel process enable the strategy to efficiently pattern the films and devices with feature size down to micrometers, equivalent to a resolution of over 1 K ppi. However, achieving uniformity over a large area remains a significant challenge for transfer patterning technology in industrial applications [56]. Beam writing is a programmable pattern generation method using micro-sized molecular beams, droplets, scanning probes or energy beam (electron, laser and ion). Despite achieving high resolution of over 1 K ppi and multiplexed beams for high speed patterning, the writing process typically bears intrinsic serial nature with low yield [57–59].

Bottom-up strategy with autonomous formation of molecules into patterns and structures are also investigated. The organic units self-assemble on various substrates, ranging from single crystalline metals to inorganic semiconductors and oxides. For example, a crystallization-mediated for the spontaneous formation of highly aligned periodic structures in organic semiconductor thin films was demonstrated [60]. Fine and complex structures can be achieved by modulating the molecule-molecule and molecule-substrate interactions, with feature size even down to molecular level [61,62]. One of the obstacle for the application of bottom-up method in organic electronics is addressing the structures by external circuits [63].

When employed without deteriorating the functionalities of the organic semiconductors, photolithography becomes an ideal patterning technique in consideration with resolution, uniformity and yield. The top-down assisted bottom-up strategy might open up a promising way to overcome the functionality deterioration problems [64]. Using pre-patterns fabricated by top-down methods like photolithography, the materials to be patterned can be directed or guided to be selectively grown/deposited at pre-designated areas. The top-down assisted bottom-up method has been widely used in carbon nanotube, inorganic semiconductor and metal system for patterning, dislocation suppression and device fabrication [65–69]. In the last two decades, the strategy was also applied to organic semiconductors with either adsorption-desorption or diffusion-binding mechanisms, showing the versatility to control over resolution, structure and size by using chemical or physical

templates [70–74]. With the strategy, high quality organic single crystals were selectively grown in patterned micro-channels in molten state or solutions [75–77].

In this review, we summarize our efforts since 2007 to develop a photolithography compatible technique for patterning small molecule organic semiconductors. The strategy takes advantage of organic molecule diffusing on substrate surface and nucleation at pre-designated locations, realizing high resolution patterning of organic materials. In addition, hetero-patterning, physical property tuning and anisotropic growth on surfaces can be achieved by manipulating with molecule-template-substrate interaction, hierarchical templates and growth parameters. Furthermore, ultra-high resolution microelectronic and optoelectronic device arrays are demonstrated with the photolithography compatible technique. Finally, a conclusion and outlook of the further developments of the technique are provided.

2. Area selective growth of organic molecules on pre-patterned surfaces

2.1. Concept, pre-pattern fabrication and molecules used in the study

Conventionally, inorganic semiconductor device processing follows "film growth and surface patterning" procedure, typically utilizing photolithography as a surface patterning technique. For organic semiconductor devices, avoiding the exposure of the materials to UV light and organic solvents poses a big challenge when employing direct photolithography for patterning. Here we conceptually overturn the conventional procedure to "surface patterning and patterned growth" for organic materials, as illustrated in Fig. 2 [78]. The substrate surface is firstly patterned by lithography when the organic materials are not presented yet. Then, the organic semiconductor molecules are deposited, which can diffuse on surface and selective nucleate at designated areas, thereby resulting in pattern formation and device fabrication on substrates.

The pre-patterns used in the studies were typically fabricated by standard resist spin-coating, baking and selective exposure to UV light through a shadow mask or electron beam scanning over surface. After pattern formation on the resist by development, the samples were typically coated with an adhesion layer and Au layer by thermal evaporation. Followed by lift-off in solvent and cleaning in de-ionized water, the patterns are formed on substrate such as SiO_2 and indium tin oxide (ITO) covered glasses for different purpose, and used as templates for the patterned growth.

Fig. 3 lists chemical structure of the organic semiconducting molecules employed in the investigation of the patterned growth. According to the morphology formed on substrates, the molecules can be categorized into non-planar molecule, planar molecule and molecule with liquid behaviors. Specifically, the diferrocene (DiFc) contains two ferrocenyl groups bridged by an oligoethylene chain [79]; the N,N'-bis-(1-naphyl)-N,N'-diphenyl-1,1'-biphenyl-4,4'-diamine (NPB) is a blue light-emitting, classic hole transport material widely used in OLEDs [16]; the 1,6-Bis(2-hydroxyphenol)pyridinel boron bis(4-*n*-butyl-phenyl)

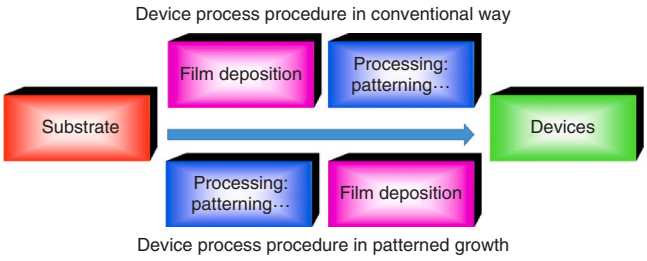

Fig. 2. Schematic of device processing procedures in conventional way and area selective growth. Adapted with permission from ref. [78]. Copyright 2012 American Chemical Society.

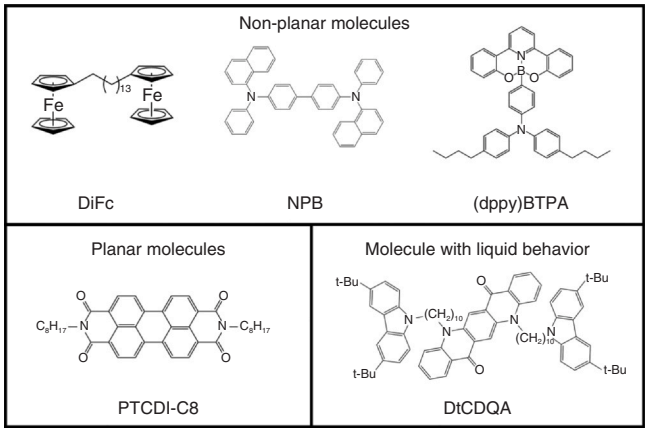

Fig. 3. Chemical structure of the molecules used in the study.

phenyleneamine ((dppy)BTPA) combines the light-emitting center with hole- and electron-transporting groups into one molecule, thus demonstrating a promising green/yellow light-emitting material [80]; the N,N-Dioctyl-3,4,9,10-perylene tetracarboxylic diimide (PTCDI-C8) is a typical n type organic semiconductor in planar configuration, with electron mobility on the order of 1 $cm^2/V.s$ [81]. N,N'-Di[(N-(3,6-di-tert-butyl-carbazyl))n-decyl] quinacridone (DtCDQA) is a high quantum yield, orange light-emitting material exhibiting liquid behavior at elevated temperature [82].

The non-planar molecules, such as DiFc, NPB and (dppy)BTPA, form dome-shaped islands that are randomly distributed on inert substrate surfaces like SiO_2, due to weak van de Waals molecule-molecule interaction. In contrast, the planar configured molecules like PTCDI-C8 can form layered films owing to the extended π system. Some non-planar molecules, e.g., DtCDQA, further exhibit liquid behavior such as anisotropic wetting on structured surface when deposited on surface at elevated substrate temperature. The atomic force microscope (AFM) images of the three categories of the molecules are summarized in Fig. 4.

2.2. Binding energy difference induced selective growth

Fig. 5a schematically shows the concept for the selective nucleation of non-planar molecules, which the substrate surface is partially patterned with materials on which the organic molecules have different binding energies from the substrate. On the left part of the substrate surface without pre-patterns, the molecules aggregate together to form randomly distributed islands. On the right part of the substrate, the molecules may prefer to nucleate on the patterned area rather than substrate owing to the larger binding energy with the pattern materials, analog to defects in a crystal surface that act as nucleation centers during film growth in atomistic model.

The binding energy difference induced selective growth was experimentally confirmed by depositing of DiFc molecules on Au patterned SiO_2, as shown in AFM image of Fig. 5b. At a substrate temperature of 45 °C, randomly distributed islands spaced in micrometers are observed, indicating a large diffusion length of the molecules on SiO_2 surface. In the patterned region, all the DiFc islands present exclusively on Au, confirming the complete selectivity of the molecule nucleation [83]. The generality of the mechanism is further demonstrated with different functional organic light-emitting molecules grown on patterned surfaces. By adjusting the dimension of pre-pattern dimensions (shape, size and periodicity) and growth parameters (substrate temperature and growth rate), the (dppy)BTPA, NPB, and DtCDQA can be deposited on pre-defined Au dot, ring and line patterns on SiO_2 with full nucleation site control, as shown in fluorescence microscope images in Fig. 5c with blue dots, green rings, and orange lines, respectively.

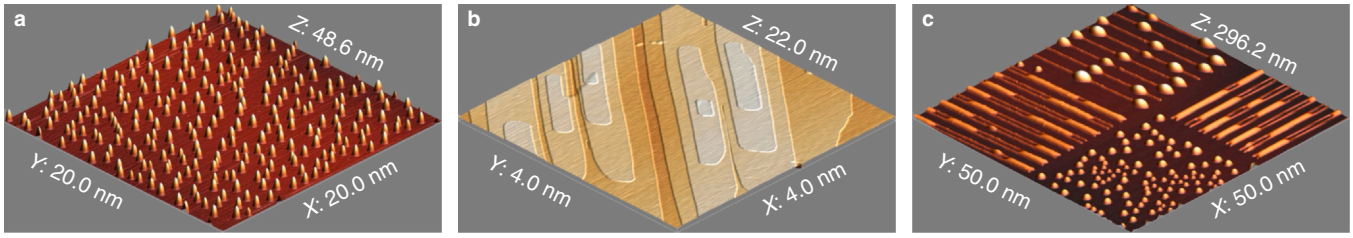

Fig. 4. 3D AFM images of a) NPB, b) PTCDI-C8 and c) DtCDQA grown on bare and Au lines patterned SiO_2. The non-planar molecule NPB and planar molecule PTCDI-C8 exhibit dome-shaped islands and layered film, respectively, when deposited onto bare SiO_2 surface. The DtCDQA molecule shows droplet-shaped islands on bare SiO_2 and liquid like behavior on structured surfaces with anisotropic wetting.

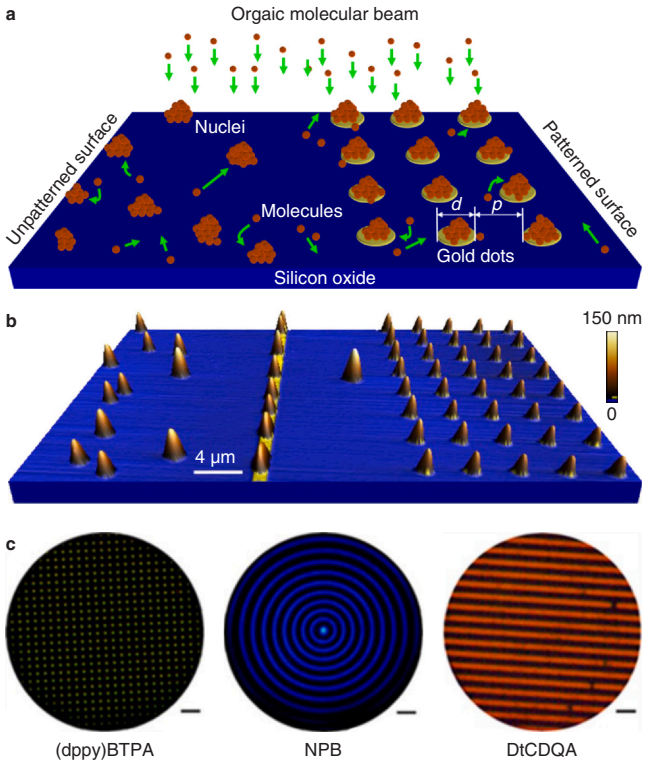

Fig. 5. Binding energy difference induced area selective nucleation of non-planar organic molecules. a) Schematic diagram, b) 3D AFM image of DiFc deposited on partial Au dots patterned SiO_2. Adapted with permission from ref. [83]. Copyright 2007, American Physical Society. c) Fluorescence microscope images of the (dppy)BTPA, NPB, and DtCDQA deposited on Au dots, rings and lines patterned SiO_2; scale bar: 5 μm.

2.3. Step-edges induced selective growth

For the planar molecules of PTCDI-C8, thin films by vacuum deposition exhibit a morphology with well-defined molecular layers, which is very different from those of non-planar molecules (Fig. 4). X-ray diffraction measurements revealed that the PTCDI-C8 molecules are oriented with the long axis of the perylene diimide core nearly vertical to the substrate surface, with molecular layer of 2.08 nm in height. When deposited onto patterned surfaces, the molecules selectively grew at the lower part of the surface. The geometry and material of the patterns have little impact on the nucleation selectivity of the molecules, as shown in the AFM images of SiO_2 dots and Au lines patterned SiO_2 (Figs. 6a and 6b). The growth of the PTCDI-C8 took place at lower part of the surface, regardless the pattern materials being SiO_2 or Au. Even when the thickness of organic layer exceeds the height of the patterns, no obvious molecules grown on top of the pre-patterns were observed.

The mechanism can be schematically interpreted in Figs. 6c and 6d, which the step edges of the pattern play a vital role. The step edges provide preferential sites for the nucleation of the molecules, similar to nucleation of atoms at atomic step edges or kinks widely observed in molecular beam epitaxy. Microscopically, the molecules will attach to the pattern edges by upright standing, providing new nucleation sites for the subsequent molecules from deposition. The strong π-π stacking of perylene diimide cores leads to lateral growth and formation of terrace domains (Fig. 6c). Further deposition of molecules will either enlarge the domains in size or pile up with formation of new molecular layers. The layered growth of PTCDI-C8 also provided a flat surface, which would maximize the fully overlapping of perylene cores to ensure selective growth of the molecules on the PTCDI-C8 area (Fig. 6d) [84].

2.4. Surface molecular density modulation induced positioned growth

As shown in Fig. 4a and 4c, non-planar molecules form randomly distributed aggregates on a bare SiO_2 surface. Microscopically, when molecules are deposited onto a homogeneous surface, they continue to diffuse until several molecules gather together to form an aggregate. Intuitively, controlling the position of aggregates is challenging due to the random walk of molecular trajectories. However, the prerequisite for aggregate formation is the local gathering of molecules to reach a critical density [85]. Assuming a surface with periodic patterns, with which the molecules have higher binding energy, the diffusing molecules will nucleate on the patterns, resulting in a spatially periodic density distribution. In principle, molecules have the highest nucleation probability at regions with maximum concentration, leading to positioning of aggregates.

The experimental validation of the idea was demonstrated by deposition of NPB on Au line grid patterned SiO_2, as shown in scanning electron microscope (SEM) images in Fig. 7a-7c. When the grid spacing is much larger than the diffusion length of molecules, several molecular aggregates are present in the middle region of the grid (Fig. 7a). The number of aggregates in each grid cell decreases with the grid spacing. As the grid spacing approaches the molecule diffusion length, only one aggregate positioned in center of each grid is observed, as shown in Fig. 7b. Further decrease of the grid spacing leads to area selective growth of molecules that completely nucleate on Au lines (Fig. 7c). Under optimized conditions, including the grid spacing, substrate temperature and growth rate, the only one molecular aggregate positioned at the center of each grid cell can be achieved with various non-planar molecules, as shown in AFM (Fig. 7d) and SEM (Fig. 7e) images of DtCDQA deposited an Au grid patterned SiO_2 surface. A statistical analysis of the AFM images was further performed by defining an X–Y coordinate system to record the aggregate position. With around 1000 grid cell in total, more than 95 % of the aggregates are located exactly on the center of the cell, as shown in Fig. 7f [86].

2.5. Kinetic Monte Carlo simulations

The patterned growth involves process of adsorption, diffusion, nucleation and desorption of deposited organic molecules on surfaces, as schematically depicted in Fig. 8a. Theoretically and numerically, the

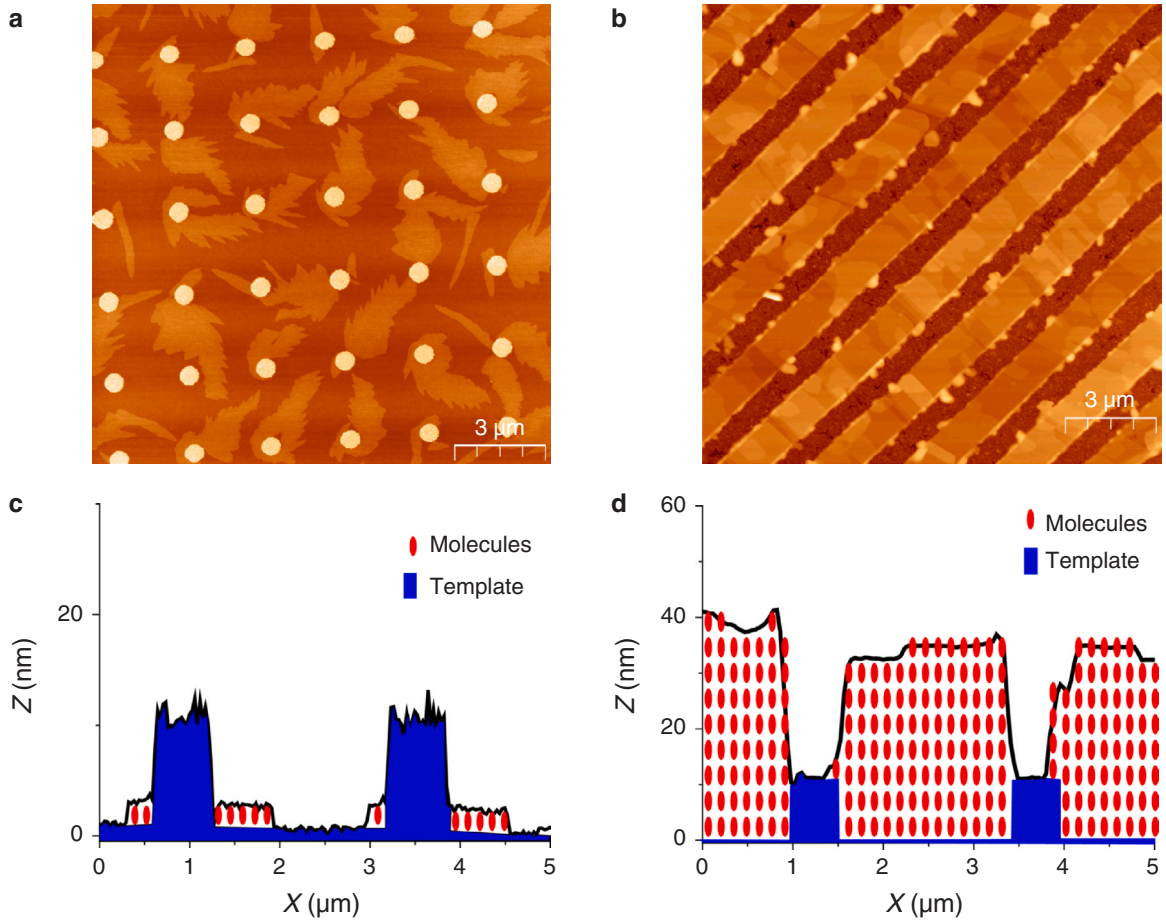

Fig. 6. Topographic AFM images of PTCDI-C8 grown on a) SiO_2 dots patterned with SiO_2 with a coverage of 0.5 ML and b) Au lines patterned SiO_2 with a coverage of 20 ML; c, d) Schematic representations of the molecules forming the observed topographic features. Adapted with permission from ref. [84]. Copyright 2009, Wiley-VCH Verlag GmbH.

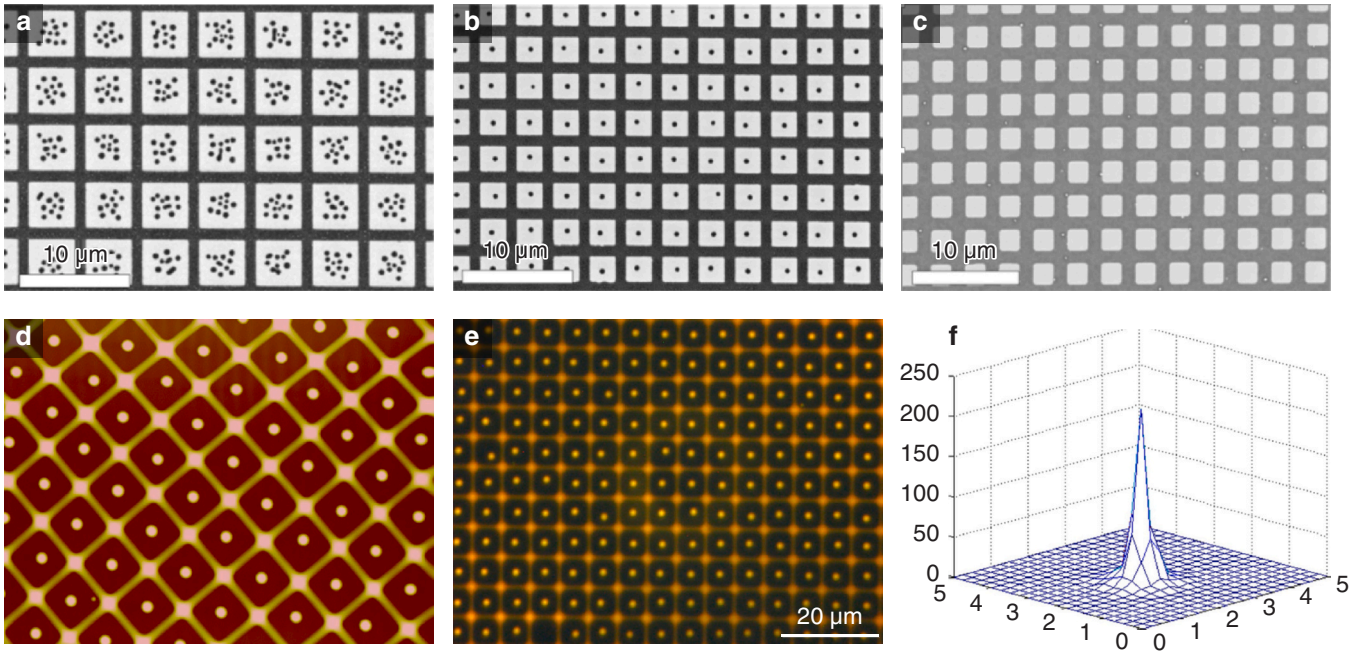

Fig. 7. a-c) SEM images of NPB deposited on (a) 4.0 μm, (b) 2.2 μm, and (c) 1.8 μm Au grid patterned SiO_2 surface. d) AFM and e) fluorescence microscope images of DtCDAQ grown on a 5 μm Au grid patterned SiO_2 surface, f) statistical cartogram of the DtCDQA aggregate position distribution. Adapted with permission from ref. [86]. Copyright 2016, Institute of Physics Publishing.

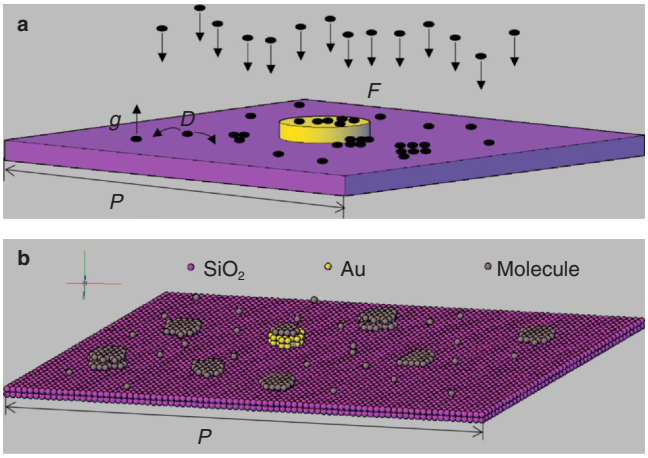

Fig. 8. a) Schematic mechanism of the area difference in binding energy induced area selective growth, b) typical simulation setup for Au dots pre-patterned SiO_2 surface. The spheres colored in pink, yellow and gray represent SiO_2, Au and molecules, respectively.

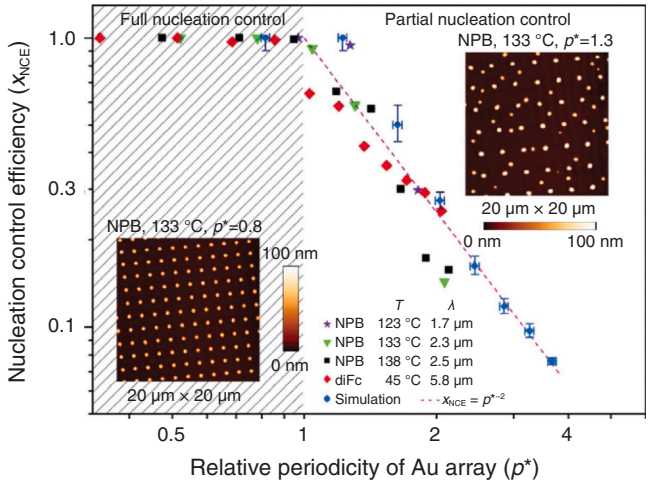

Fig. 9. Relationship of the nucleation control efficiency χ_{NCE} and the relative periodicity p* from MC simulations and experiments. A full control of nucleation $\chi_{NCE}=1$ can be achieved when $p^* < 1$; the χ_{NCE} is gradually decreased to follow $\chi_{NCE}=p^{*-2}$ as $p^* > 1$. Insets are AFM images of NPB grown on Au dots patterned SiO_2 at $p^*=0.8$ (left) and $p^*=1.3$ (right), respectively. Adapted with permission from ref. [83]. Copyright 2007, American Physical Society.

behavior can be modeled by *Monte Carlo* (MC) simulations, which provide statistical results from a large number of random samples [87]. Specifically, the kinetic MC is extensively employed to model the temporal evolution of atoms and molecules diffusing on surfaces. In the modeling, the material system is treated as distinct spherical particles representing substrate (S), patterned materials (A) and deposited molecules (M), respectively. The Lenard-Jones (LJ) pair potentials are applied to mimic the van de Waals interaction between particles using the equation [83]:

$$V(r) = 4\epsilon\bullet\left[\left(\frac{\sigma}{r}\right)^{12} - \left(\frac{\sigma}{r}\right)^{6} + (r - r_c)\left(\frac{12\sigma^{12}}{r_c^{13}} - \frac{6\sigma^{6}}{r_c^{7}}\right) + \left(\frac{\sigma}{r_c}\right)^{6} - \left(\frac{\sigma}{r_c}\right)^{12}\right], for r < r_c \quad (1)$$

where the σ and ϵ are measures for the atom-atom distance and depth of the potential well, respectively. A cutoff r_c, above which the interaction energy is set to zero for simplicity, is further chosen to enhance computational efficiency.

Following optimization of periodic conditions and the interactions of particles in the system, the probability of diffusion events (p_i) can be obtained using the Arrhenius expression:

$$p_i = De^{\frac{\Delta E_b}{k_B T}} \quad (2)$$

where D is the effective vibration frequency of the particles, k_B is the Boltzmann's constant and T is the absolute temperature of the system. The diffusion barrier ΔE_b is derived from the potential energy difference between the system before and after diffusion. During each simulation step, only one MC move is selected according to the standard Metropolis criterion. Typically, averaged results from multiple simulations were used.

In the simulation model, the substrate was constructed out of long range ordered S particles with repeated unit cell on surface; the patterned material A particles are located on the substrate surface in designated morphology, as shown in Fig. 8b. To mimic the Au patterned SiO_2 substrates with which the atoms are not diffusive during the growth, the A and S particles are fixed during the simulations. In this case, the relevant interactions in the system can be reduced to those involving molecules (M) only. The deposited molecules were simulated to be randomly added to the system at a given MC steps (typically 10^4-10^6 steps), similar to the molecules evaporated from an evaporator. When the M particle moved to a distance larger than r_c, it was considered to be desorbed from the surface and removed from the system.

One of the motivations for patterned growth is to define the organic molecules at pre-determined locations, generating high resolution organic semiconductor patterns. Systematic experiments on different organic semiconductors reveal that all the molecules can be controlled to nucleate on the Au dots when the pattern periodicity is less than a characteristic length. However, the number of extra islands on SiO_2 increases with the periodicity p, as shown in the inserted AFM images of Fig. 9. For a better description, a nucleation control efficiency (NCE, defined as $\chi_{NCE}=N_{Au}/N$) and a characteristic length (λ, defined as $(N/A)^{-1/2}$) are introduced. Counted in a given surface area A which is normally the scanning field of AFM or SEM images, here the N_{AU} and N are the number of pre-patterned Au dots and the total number of the organic islands, respectively. According to the definition, the λ is a measure of distance between islands, which is determined by molecular diffusivity on surface, and relates to growth parameters such as substrate temperature T and beam flux F. To compare the different experiments and theoretical simulations, a dimensionless periodicity $p^*=p/\lambda$ is further introduced, where p is the periodicity of the pre-patterned Au dots.

The simulation system was quadratic shaped with a periodic boundary conditions, containing a close packed fcc lattice with (111) surface as substrate S, a layered dot located in the middle as patterned dot A and diffusive particles as organic molecules M (Fig. 8b). In the simulations, the interaction parameters of the Lennard-Jones potential (Eq. 1) were optimized as $\varepsilon_{MM}/k_BT=3.7$, $\varepsilon_{MA}/k_BT=5$, $\varepsilon_{MS}/k_BT=1.5$, respectively, to mimic the interaction between molecules, and the interactions of molecules with Au and SiO_2, respectively. The cut-off r_c was set as $2.5a$, where a is the distance of the nearest-neighbor atoms. After a sufficient simulation time, a quasi-equilibrium distribution of islands was obtained. The simulations reveal a p* dependent phenomenon, as shown in blue circles of Fig. 9. For $p^* < 1$, all the islands are grown on Au dots, resulting in $\chi_{NCE}=1$; additional islands located on SiO_2 start to appear when p* increase to > 1, following the rule of $\chi_{NCE}=p^{*-2}$. Shown in Fig. 9, the simulations are in good agreements with the experimental results, confirming the generality of the physical mechanism [83].

The kinetic MC simulations were successfully employed to model the patterned growth process, which is dominated by diffusive behavior over a relatively long time rather than ballistic movement over a short time [88,89]. In addition to controlling nucleation efficiency, the modulation of molecular density on a grid-patterned surface was also explored at the microscopic level for the position control of aggregates [86]. Using the kinetic MC algorithm, several groups have numerically

replicated interesting phenomena observed in experiments, such as the loss of nucleation control [90], effects of diffusion length [91], and anisotropic behaviors [92]. With a given substrate and template system, e.g. Au patterned SiO_2, the mechanism of patterned growth process is dominated by molecule-molecule interaction. The binding energy difference induced patterned growth was typically observed for nonplanar molecules, owing to the weak van de Waals interaction between molecules. In contrast, step-edge induced patterned growth was achieved with planar configured molecules, originating from lateral growth by strong π-π interaction. Attempts have also been made to explore the mechanism of step-edge-induced area selective growth [93–95]. However, the mechanism requires anisotropic interactions between molecules, posing a challenge for the MC simulation to model the system.

3. Physical dimensions and properties engineering based on patterned growth

Based on the atomistic model for thin film deposition, the deposited atoms diffuse on the substrate surface and nucleate at defects, step-edges or aggregate together, and then evolve to form stable nuclei. In combination with the surface patterning technologies and vacuum deposition, all the three nucleation mechanisms at atomic scale can be enlarged to micro-scale for high resolution organic semiconductor patterning. Furthermore, the physical dimensions and properties of the patterned structures can be engineered, providing a versatile technique to process organic functional films and devices.

3.1. Surface architecture by anisotropic wetting

Surface architecture is of significant interest for various applications in optics and electronics [96]. In microelectronics, the devices are required not only to be microscopically patterned, but also electrically addressed. The registry of devices through reading-out circuits remains a challenge for organic semiconductors, especially for the circuit that designed for high level integration. Liquids on structured surface demonstrated anisotropic wetting with formation of complex surface architecture [97]. However, the typical employed liquids, usually water and organic solvents with the high vapor pressure, are challenging to manipulate at micro/nano scale. With low vapor pressure and tunable melting point, organic functional molecules are ideal materials for microscopic control of liquids at structured surfaces [98].

Fig. 10a shows a SEM image of a 30 nm DtCDQA deposited on partially Au lines patterned SiO_2 substrate. The sample surface consists of bare SiO_2 (bottom left), a single line array (top right) and two line-pair arrays in orthogonal directions (top left and bottom right). Three different features of DtCDQA can be easily recognized for the molecules aggregated in different areas (black color in the SEM image): circles on bare SiO_2, ovals riding on single Au lines advancing towards SiO_2, and segments between Au line pairs. AFM measurements confirmed that the features are shaped as spherical caps on bare SiO_2, bulges on single Au lines, and cylinder segments on Au line pairs. Detailed analyses of contact angles revealed that the propagation of segments is mostly driven by the small contact angle along the Au lines.

The anisotropic wetting of molecules along line pairs can further be utilized to fabricate high resolution organic semiconductor crossbar structures, as shown in Fig. 10b. The substrate surfaces were patterned with two kind of structures: one is Au line array as columns; and the other one consists of four segments with an offset to each other, shown in top left of the Fig. 10b in regions without deposited molecules. With a small DtCDQA deposition amount of 3 nm, small liquid drops that reside on single Au lines and elongated drops along the segment pairs are observed. The elongated drops propagate with increased deposition amount of 10 nm, following the direction of discontinued channels defined by the segment pairs. With increasing deposition amount of 30 nm, the elongated droplets keep wetting the channels and coalesce together to form a long one. Finally, the organic cylinder segments connect each other to form a crossbar structure with deposition amount of 50 nm. The resolution of the structure is completely compatible with those obtained in inorganic semiconductors, reaching over 8 K ppi in Fig. 10b [99].

3.2. Hetero-patterning of organic functional materials

Hetero-patterning, which materials are structured both laterally and vertically, has attracted increasing attention in applications such as spectrometry, biology and optics [100]. Besides the in-plane lateral patterning, it requires an additional out-of-plane control in thickness or height. The parallel process patterning techniques like photolithography and stamp printing can normally generate lateral structures at same height over sample surfaces. Using aperturized beams of laser, ions, electrons, liquid droplets and evaporated molecules, complex 3D structures can also be printed or sculptured [101–103]. However, the

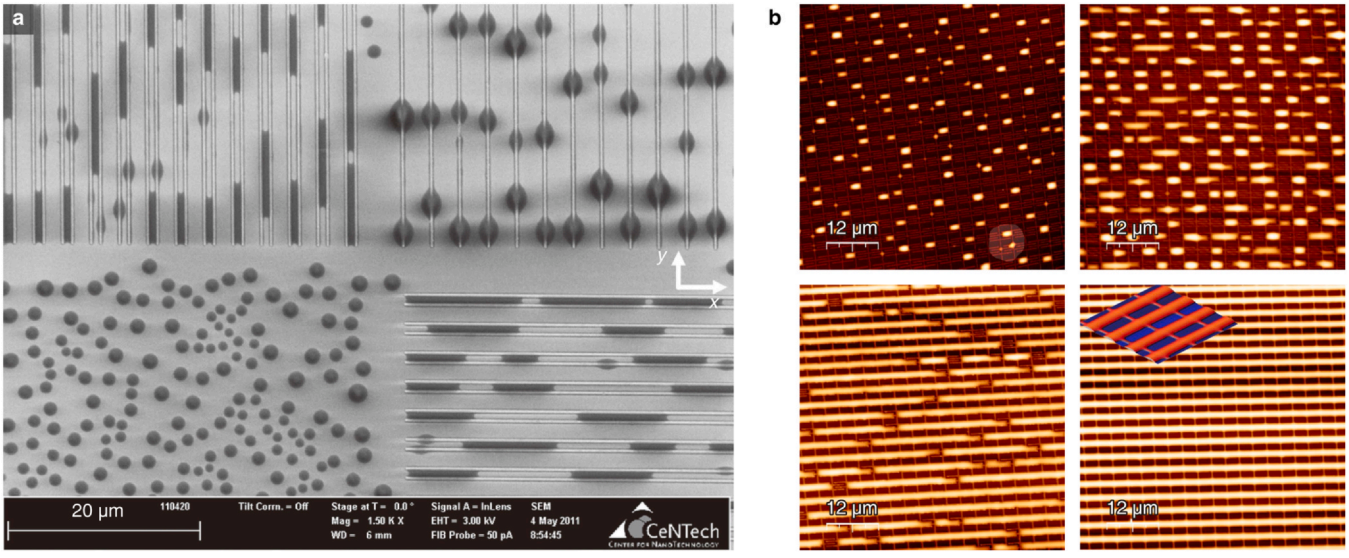

Fig. 10. a) SEM image of a 30 nm nominally thick layer of deposited DtCDQA grown on Au line-patterned SiO_2, the patterns consist of one single line array and two line-pair arrays in orthogonal directions, b) Morphology evolution of DtCDQA grown on a pre-patterned substrate to form an addressable cross-bar structure with ever increasing deposition amount of 3, 10, 30 and 50 nm, respectively. Adapted with permission from ref. [99]. Copyright 2013, Wiley-VCH Verlag GmbH.

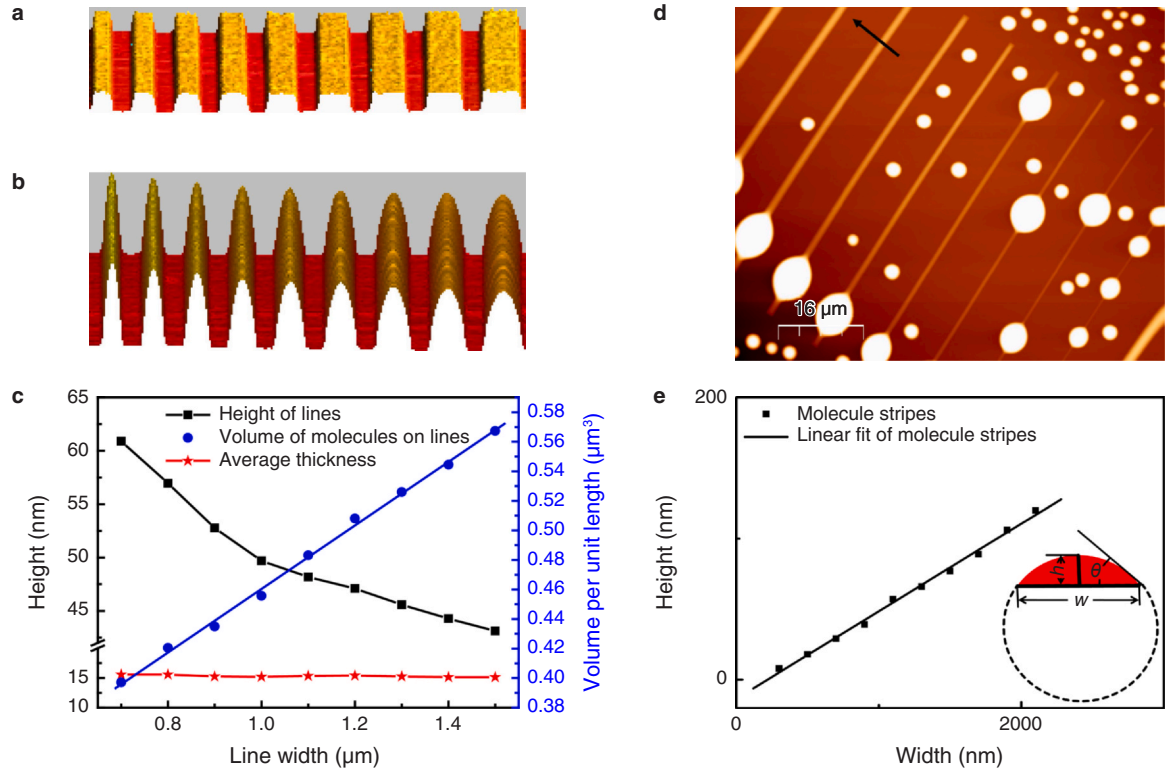

Fig. 11. 3D AFM images of a) Au lines with width increasing from 700 nm (left) to 1.5 μm (right) and spacing of 1 μm, and b) 30 nm NPB deposited on the Au lines patterned surface. c) Height, volume of molecules on each line, and average thickness of deposited molecules. Adapted with permission from ref. [78]. Copyright 2012, American Chemical Society. d) AFM image of 50 nm DtCDQA grown on Au lines patterned SiO_2. The Au line widths vary from 0.3 to 2.3 μm with 0.2 μm increments. e) heigh-width relationship of DtCDQA grown on Au lines. Adapted with permission from ref. [104]. Copyright 2011, Wiley-VCH Verlag GmbH.

inherent serial nature of these processes hinders their scalability for high yield.

Fundamentally, the patterned growth involves absorption of the diffusing molecules on pre-defined area, which further enables the modulation of volume and height of the micro-patterns. Assuming the uptake of molecules is size independent, logically the pre-defined patterns in small size should have higher height in comparison to those in large size. The concept is experimentally validated in Fig. 11a-c, with the Au line-shaped patterns generated on SiO_2 by subsequent electron beam lithography, metal vapor deposition and liftoff in solvents. The width W of the lines increases from left to right while keeping the spacing S fixed. The 3D AFM profile in Fig. 11a illustrate uniform height of 5 nm for all lines produced by the lithographical procedure. Upon deposition of 30 nm NPB, noticeable variations in the height of each molecular stipe were observed, shown in Fig. 11b. The height and volume of molecules on lines, as well as average thickness, are summarized in Fig. 11c, confirming a linear increasing in height and decreasing in volume when the W decreases. Further calculations, through dividing of the volume to effective area A (defined as $(W+S)/L$, where L is the length of the lines), revealed that the height is related to normalized thickness of the film that determined by growth rate and time. Consequently, precise control over three dimensions of surface structure can be achieved at sub-micrometer resolution, by well designing of pattern lateral dimensions, growth rate and deposition time [78].

Fig. 11d shows a 12 nm DtCDQA deposited onto Au lines patterned surface. Interestingly, the height of DtCDQA molecule increases with the line width, which is contrary to those of NPB deposited on similar surfaces. By taking the AFM cross-sectional profiles along the arrow direction in Fig. 11d, the height-width follows a linear relationship, a phenomenon widely observed when a liquid wets a chemically patterned surface. The relationship adheres the rule of $h/w = (1-\cos\theta)/\sin\theta$, where the h, l and θ are the height, width and contact angle, respectively. With given liquid and surface, normally the contact angle of θ is also fixed. The determined contact angle gives to a constant of the h/w according to the rule, resulting in a linear relationship between height and width [104]. The liquid behavior of molecule on surfaces further introduces an additional parameter of contact angle θ for the 3D structure dimension engineering.

The liquid behavior of DtCDQA on a patterned surface further enables the hereto-patterning of the structures. Using hierarchical Au dot arrays consisting of two sets of Au dots with diameter d of 0.5 and 2 μm, 12 nm DtCDQA were deposited and selectively grown on Au patterns, exhibiting two height distributions: 106.5 ± 1.3 nm on 2 μm Au dots and 118.6 ± 1.1 nm on 0.5 μm ones as shown in the top AFM image in Fig. 12a. Upon annealing at 220 °C for 12 h, the height of DtCDQA on big and small Au dots can be continuously tuned to 151.9 ± 1.3 nm and 56.8 ± 1.4 nm, respectively, as shown in the bottom AFM image in Fig. 12a [105]. Contact angles extracted from AFM data revealed that the DtCDQA on small Au dots, with a contact angle of 19.2 °, has actually advanced to the SiO_2 surface. While the DtCDQA on big dots is still confined on Au with the contact angle of 11.2 ° [99]. Hence, two liquid-solid boundaries are presented with the deposition of 12 nm DtCDQA on hierarchical Au dots patterned SiO_2 surface: large islands completely confined on the 2 μm Au dots and small islands riding on both 0.5 μm Au dots and SiO_2 surface, as schematically shown in Fig. 12b. The two boundaries further give rise to two energy barriers for molecule diffusion, which are defined as $E_{M\text{-}SiO2}$ and $E_{M\text{-}Au}$, respectively. Typically the $E_{M\text{-}SiO2}$ is weaker than the $E_{M\text{-}Au}$ owing to the strong interaction of molecule with metals. When annealed at a mediate temperature denoted as T_2 in Fig. 12b, the molecules on SiO_2 can overcome the energy barrier of $E_{M\text{-}SiO2}$, escaping from the islands riding on small Au dots and SiO_2 and diffusing on surface again. Some molecules may diffuse to the island on big Au dots, leading to an increased island height on big Au dots and decreased height on small ones. As a result, the island height on both big and small dots can be continuously tuned with annealing time, as shown in Fig. 12c, giving a temporal control of the dimension in the out-of-plane direction [105].

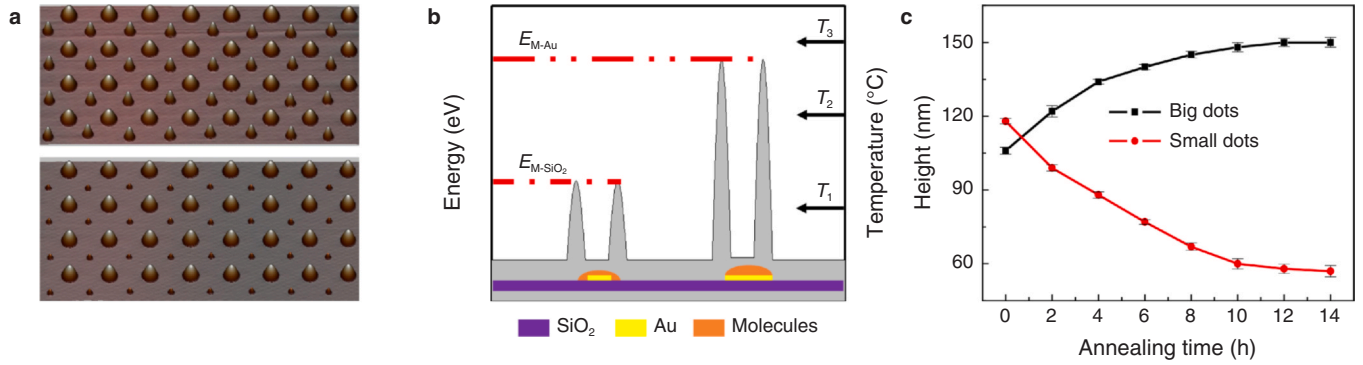

Fig. 12. a) 3D AFM images of 12 nm DtCDQA deposited on hierarchically Au dots patterned SiO_2: as grown (top) and annealed at 220 °C for 12 h (bottom). b) Schematics of organic islands on big and small Au dots and corresponding energy diagram. c) Temporal height evolution of the big and small DtCDQA islands at an annealing temperature of 220 °C. Adapted with permission from ref. [105]. Copyright 2014, Wiley-VCH Verlag GmbH.

3.3. Tunable single-, bi- and multi- color patterning

Color patterning is crucial in sensors, imaging and displays, ideally with tunability in emission wavelength and monolithic integration of full colors [106]. Conventionally full color integration is achieved by subsequent defining different materials on a single substrate [107]. However, creating multi-color patterns with feature sizes down to micrometers remains a challenge for organic functional materials. The employed techniques such as shadow mask and inkjet printing suffer limitations in either resolution or yield. With the nucleation control strategy, the tunable single-, bi- and multi-color patterns can be maskless realized by combing co-deposition of two kinds of molecules and hetero-patterning techniques.

Fig. 13a illustrates the fabrication of tunable single color pattern by area selective growth with co-deposition of NPB and DtCDQA. The both molecules were evaporated from two independent sources and co-deposited onto the Au dots patterned SiO_2 with different mixing ratio, as shown in the schematics. The AFM measurements reveal that the both molecules can diffuse to nucleate on Au area, when the periodicity of the Au dot array is less than the characteristic length λ defined in Fig. 9. Fluorescence microscope characterization further demonstrates that the emission color of the organic structure is strongly DtCDQA/NPB mixing ratio dependent. The color can be tuned from deep blue to green and then to orange, as the concentration of DtCDQA in NPB increased from 0 % to 10 % and then to 100 %. Photoluminescence measurements on the samples confirmed a green emission peaked at 527 nm were observed in co-deposited samples with low DtCDQA concentration. This green emission originates from DtCDQA monomer when surrounded by NPB. Together with the blue emission from pure NPB and orange

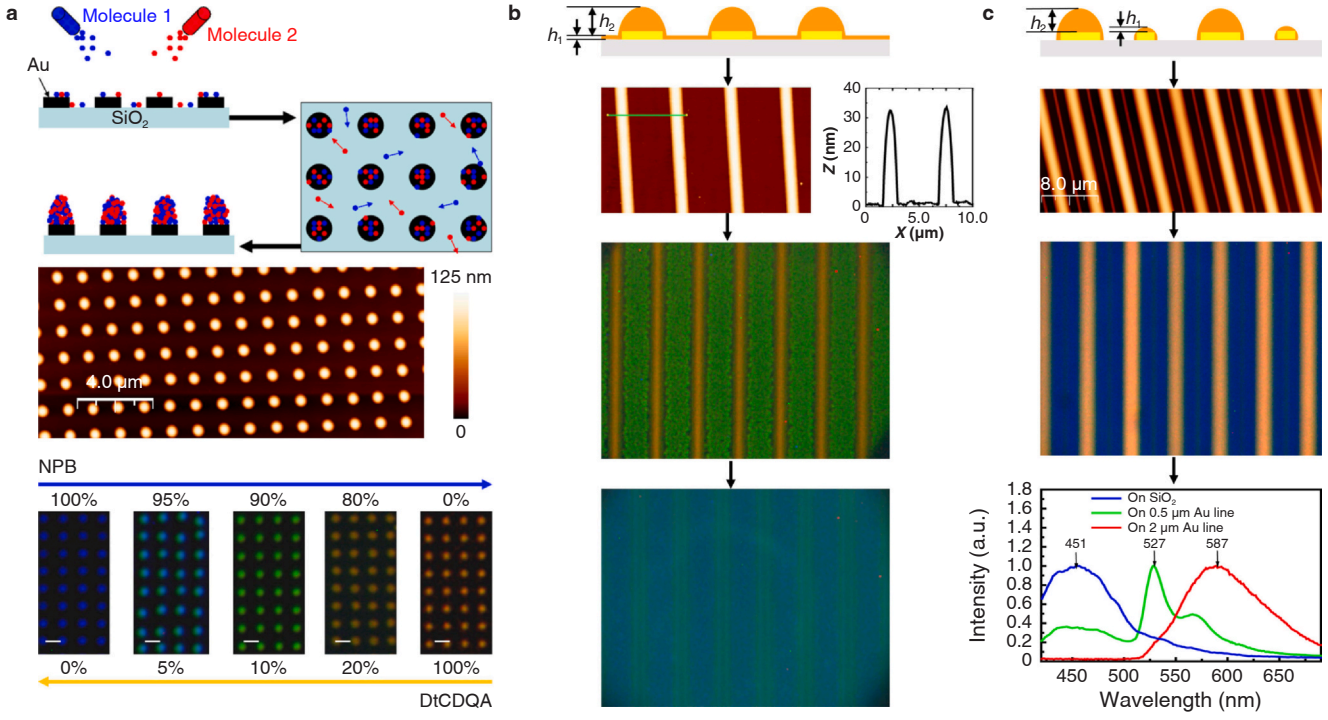

Fig. 13. a) Schematic evolution of patterned growth with two molecules on a patterned substrate, AFM image of co-deposited NPB and DtCDQA at mixing ratio of 9:1 and fluorescence microscopy images of co-deposited NPB and DtCDQA with different mixing ratio. b) Schematic representation of DtCDQA distribution on a patterned surface using a two-step growth technique, AFM images of 5 nm DtCDQA grown at 180 °C followed by 1 nm DtCDQA at 50 °C on an Au line array patterned SiO_2, resulting h1 of 32 nm and h2 of 1 nm shown in corresponding AFM profile, and fluorescence microscopy images of upon deposition of 10 nm and 100 nm NPB at 100 °C, respectively. Adapted with permission from ref. [108]. Copyright 2010, Wiley-VCH Verlag GmbH. c) Schematic representation of DtCDQA hetero-pattern grown on hierarchical Au line array patterned surface, AFM image of 30 nm DtCDQA grown on alternating 0.5 and 2 μm hierarchical Au lines patterned on SiO_2 with spacing of 1 μ m, fluorescence microscopy image of 150 nm NPB deposited on the DtCDQA hetero-pattern and photoluminescence spectra of the corresponding colors. Adapted with permission from ref. [104]. Copyright 2011, Wiley-VCH Verlag GmbH.

emission from DtCDQA aggregate, blue, green and orange emissions can be realized only with two kinds of molecules. The relative intensity of the three emissions varies with the mixing ratio, resulting in the tunable color patterns [108].

The DtCDQA/NPB ratio dependent photoluminescence emissions further enable to achieve tunable bi-color patterns on hetero-patterns, as shown in Fig. 13b. The hetero-patterns were fabricated by a two-step growth with different substrate temperature, achieving h1 on SiO_2 and h2 on Au. Firstly a high substrate temperature was used to grow DtCDQA molecules selectively on Au area; and then low substrate temperature was employed to uniformly coat the samples with a thin DtCDQA layer. Taking the Au lines (width of 1 μm and periodicity of 5 μm) on SiO_2, the h1of 1 nm and h2 of 32 nm can be obtained by optimizing the substrate temperate and deposition amount in each step. A subsequent deposition of 10 nm NPB on the DtCDQA hetero-patterned sample leads to 10 % and 76 % of DtCDQA concentration on SiO_2 and Au areas, respectively. The difference in DtCDQA concentration in NPB gives an orange-green bi-color pattern. In addition, the orange-green bi-color patterned can be tuned to green-blue one by further deposition of 100 nm NPB, diluting the DtCDQA on Au area into monomer emission and switching the NPB as dominant emission on SiO_2 [108].

The liquid behavior of DtCDQA provides additional parameter, by means of contact angle, for control over hetero-patterns and fabricating tipple-color patterns, as shown in Fig. 13c. With hierarchical Au lien arrays (alternating 2 μm and 0.5 μm Au lines spaced by 1 μm), hetero-patterns were achieved by depositing 30 nm DtCDQA, resulting in h2 of 120 nm on wide Au stripes, h1 of 22 nm on narrow Au stripes and no molecules on SiO_2. Further deposition of 150 nm NPB onto the sample created a DtCDQA concentration of roughly 45 % on the 2 μm Au lines, 12 % on the 0.5 μm Au lines and 0 % on the SiO_2, respectively. Accordingly, the fluorescence characterization of the sample exhibited an orange-green-blue triple color pattern, in corresponding to DtCDQA aggregate, DtCDQA monomer and NPB, respectively [104]. Photoluminescence spectra obtained on the location further confirmed the origin of the emissions. Certainly, tunable multicolor (more than three) patterns can also be realized by optimizing the pre-pattern dimensions and deposited molecule amount.

3.4. Multi-species micro-patterning

Multi-species micro-patterning, which various materials are spatially arranged at the micrometer scale, plays a critical role in applications such as optoelectronics, microelectronic and displays. For instance, full color micro-displays require precise patterning of materials that emit red, green and blue light [109]. Efficiency of organic solar cells benefits significantly from the phase separation of p- and n-type materials, facilitating effective exciton separation and carrier capture at the interface [110]. By employing the patterned growth strategies that induced by either binding energy difference, step-edges or molecular density modulation, organic molecules can be controlled to grow on designated locations. The control over growth location opens up new possibilities for patterning multi-species materials by combining different patterned growth mechanisms.

Fig. 14a shows 3D AFM images (bottom) and schematic representations (top), illustrating microscale separation of PTCDI-C8 and NPB. When PTCDI-C8 was deposited onto an Au dot array patterned SiO_2 at optimized substrate temperature, molecules nucleate at Au step edges and laterally grow on SiO_2. A PTCDI-C8 wetting layer may also be formed on Au surface during the deposition, revealing different orientation of molecules: with the perylene diimide core parallel to the Au surface and vertical to SiO_2, as shown in middle schematic of Fig. 14a. The different orientation of perylene diimide core further creates a binding energy difference for NPB upon deposition. Consequently, NPB molecules will diffuse on PTCDI-C8 vertical oriented area owing to the inert alkyl surface and nucleate on parallel perylene core with relatively strong interaction, resulting in selective growth of NPB on Au area. Hence, microscale molecule separation can be achieved: PTCDI-C8 on SiO_2 and NPB on Au, shown in the 3D AFM image and schematic representation in the right of Fig. 14a [84].

In addition, the surface molecule density modulation and binding energy difference induced position control can also be combined to achieve multi-species micropatterning for organic molecules, as illustrate in the fluorescence microscope images (bottom) and schematic representations (top) in Fig. 14b. When DtCDQA molecules deposited on Au grid pattern surfaces with periodicity $p > \lambda$, selective growth on Au and extra nucleation on SiO_2 took place, as shown in fluorescence microscope image in the left part of Fig. 14b. Taking advantage of molecule diffusion barrier $E_{M\text{-}SiO2} < E_{M\text{-}Au}$ (see Fig. 12b), the DtCDQA molecules in the extra aggregates on SiO_2 can be removed by annealing at a moderate substrate temperature, which activates the molecules diffusing to Au area, as shown in middle of Fig. 14e. Subsequent deposition of a small amount of NPB leads to a surface molecule density modulation induced aggregate position control at center of the grid. During the formation of NPB islands, a few diffusing DtCDQA molecules aggregate together with the NPB, producing bi-color pattern with orange aggregate emission on Au and green monomer emission in grid center (right of Fig. 14b) [111].

3.5. Orientation control of patterned organic crystalline films

Crystalline organic thin films typically demonstrate orientation dependent properties, which relates to extent of π-π stacking. For

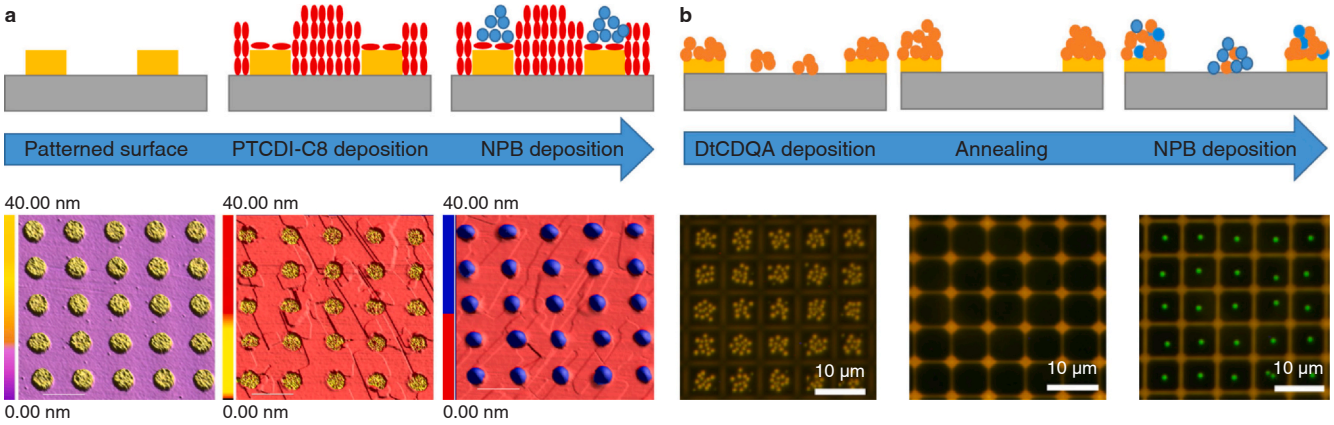

Fig. 14. a) Schematic representations and AFM image of PTCDI-C8 and NPB separation: Au dots patented SiO_2 (left), upon deposition of PTCDI-C8 (middle), and subsequent deposition of NPB (right). Adapted with permission from ref. [84]. Copyright 2009, Wiley-VCH Verlag GmbH. b) Schematic representations and fluorescence microscope images of DtCDQA and NPB separation: 6 nm DtCDQA deposited on Au grid patterned SiO_2 (left), annealing for 2 h at moderate temperature (middle), and subsequent deposition of 1.2 nm NPB (right). Adapted with permission from ref. 111. Copyright 2017, Royal Society of Chemistry.

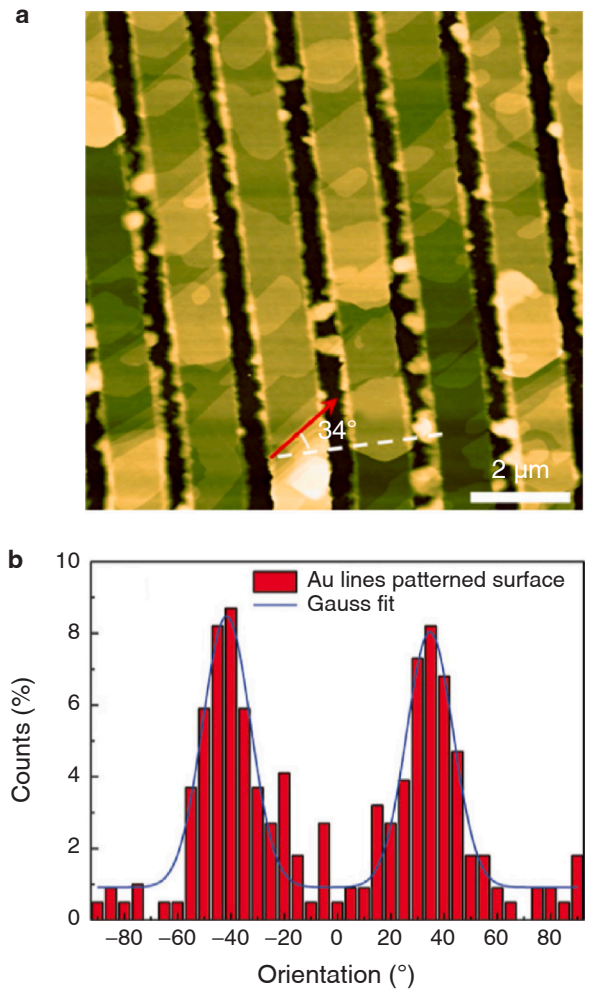

Fig. 15. a) AFM image of 30 nm PTCDI-C8 deposited on SiO_2 substrate with Au lines. The red solid arrow indicates the orientation of the corresponding PTCDI-C8 stripe, while the white dash line are drawn to indicate the direction perpendicular to the Au lines. b) Orientation distribution of PTCDI-C8 grown on Au lines patterned SiO_2. Adapted with permission from ref. [117]. Copyright 2023, Wiley-VCH Verlag GmbH.

instance, variation in carrier mobility up to one order of magnitude was observed for different orientation of 6,13bis(triisopropylsilylethynyl) pentacene crystalline films [112]. Micro-crystals grown on dielectric layers, such as SiO_2, typically exhibit a random distribution of orientations. Attempts to achieve orientation control of organic crystalline films were extensively explored with a certain success, including employing the external forces, light, magnetic and electrical fields as stimulus to modulate the molecular orientation [113–115]. Analog to molecular beam epitaxy, molecular templates also have a great impact on the orientation of organic films upon deposition [116].

When deposited on Au lines patterned SiO_2 surfaces, PTCDI-C8 films were patterned with an aligned orientation, shown in the AFM image of Fig. 15a. To quantify the distribution of the orientation, reference lines vertical to the Au stripe (white) and along the organic film terrace (red) are marked, defining an orientation angle φ. Statistics distribution of the orientation angle φ over 1000 PTCDI-C8 stripes reveals two obvious maximums that peaked at −41° and 35 °, shown in Fig. 15b. Microscopically the orientation aligned film growth was speculated as the PTCDI-C8 molecules first attach to Au step edges with perylene diimide cores vertical to SiO_2 surface, providing nucleation sites for directional growth along the a-axis of the molecule crystal owing the strong π-π stacking between molecules [117] The observed broad distribution of the orientation angle was attributed to the roughness of the pattern (estimated to about nanometers), which leads a directional fluctuation of perylene diimide core planes when absorbed to the step edges. We believe the finding provides an alternative strategy to grow oriented crystalline films for high device performance uniformity.

4. Template assisted patterning of functional materials in non-vacuum environments

The patterned growth by vacuum deposition utilizes pre-patterns (templates) as nucleation sites for diffusing molecules under vacuum conditions, providing a versatile way for high resolution thin film patterning and engineering. However, the process is strictly limited to sublimable materials such as small molecular organic semiconductor, with relatively high instrument maintenance cost. An extension of the material to other function materials such as polymers and quantum dots is desirable, ideally in non-vacuum environments.

4.1. Patterning and transporting organic materials by selective wetting

Selective wetting of water on chemically or morphologically textured surfaces has been extensively investigated in both scientific and industrial interest [118]. Very similar to patterned growth by selective nucleation control, selective wetting can also be employed to confine materials on defined areas, directly in atmosphere circumstance. For demonstration, N-ethyl-d-glucamine (NEDG) with its chemical structure shown in Fig. 16a, was chosen owing to no significant carbonization above its melting point in air. In the molten state, the NEDG can progress along the Au stripes that lithographically patterned on SiO_2, as schematically illustrated in Fig. 16b. The SEM images on temporal evolution of NEDG wetting on stripes show a width dependent wetting distance (Fig. 16c-16e). The relationship of distance of molecules wetting on Au stripes L and time t follows a universal diffusion law $L \sim t^{1/2}$, which the diffusive mechanism was confirmed by existence of a thin precursor layer at the microscopic liquid front [119]. Besides patterning molecules directly in air, the selective wetting method can further be employed as host to transport other functional materials, such as dye molecules, to create bi- and tri-color patterns.

A key process for the manipulating molten molecules on surface is to confine the thermal activated precursor layer inside the patterned area. This gave us a hint that when thermal heating is locally activated by electrical field, an electrically driven surface microfluidics could be realized without mechanical pumps and valves. Fig. 16f shows the micro-flow of molten wax on Au-patterned glass surfaces with a driving voltage lower than 10 volts. The selective heating of each Au stripe (surface channel) is activated by Joule heating produced by electrical current passing through the Au layer. When applied a voltage on electrodes, the corresponding surface channel will be heated up to reach a temperature above the melting point of the wax, while the temperature of the other channels remains below wax melting point [120]. The wax molecules on heated up channel were activated to propagate along the open surface channels, performing complicated micro-flow control over predesigned paths, including substance transporting and serial diluting without pumps and valves.

4.2. Transfer printing of liquid droplets by selective de-wetting

Selective de-wetting on patterned surfaces has also been developed as a method to define functional materials on surfaces. For instance, on a hydrophobic/hydrophilic patterned surface, a solution containing substances de-wets from the hydrophobic region and wets the hydrophilic features. The substances deposit on the hydrophilic features after solvent evaporation [121]. The method was employed to pattern various materials including organic semiconductors and quantum dos for fabrication of microelectronics and optoelectronics [122]. Typically, the patterned substrates were used only once for pattern formation or device

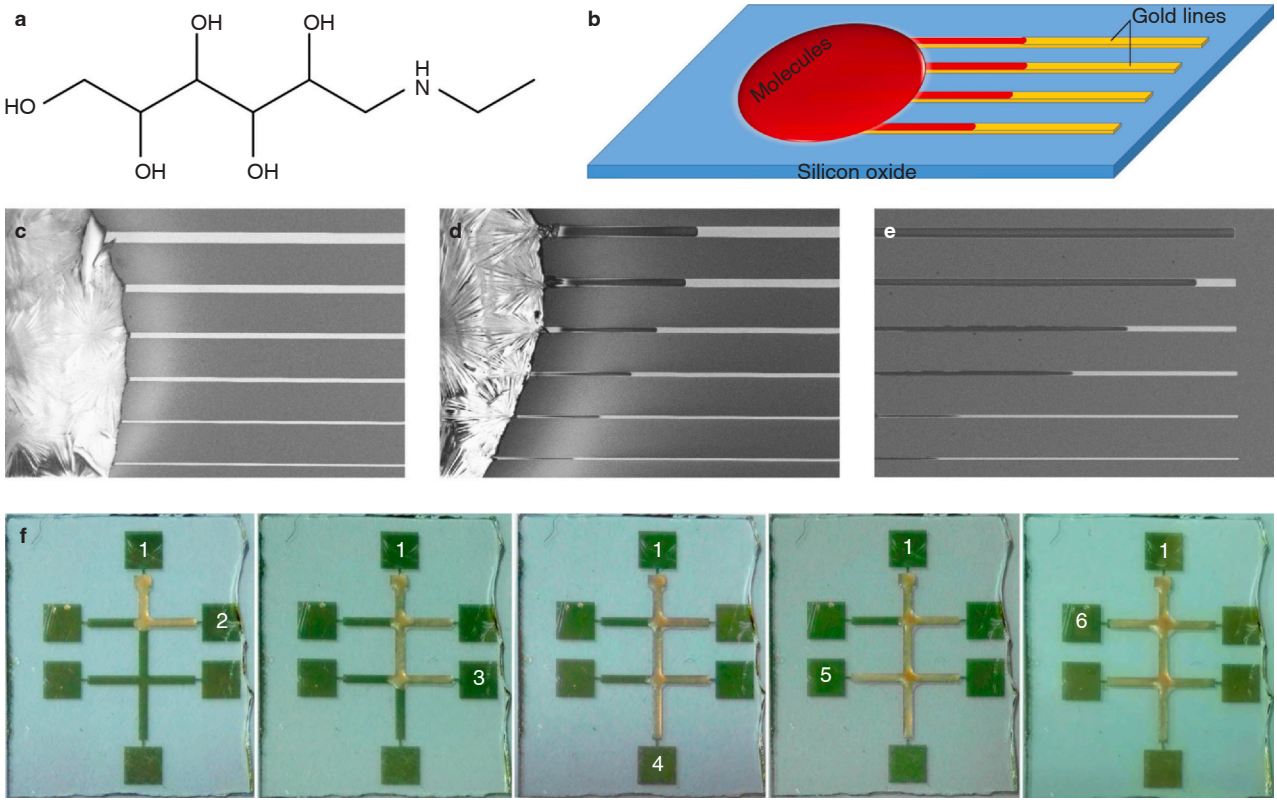

Fig. 16. Molecular structure of NEDG. b) Schematic diagram of surface microfluidic patterning of NEDG molecules. c) Temporal evolution of NEDG on Au stripe-patterned SiO_2 at 0, 1 and 10 min, respectively. Adapted with permission from ref. [119]. Copyright 2014, Wiley-VCH Verlag GmbH d) Selective wetting of the molten wax on Au patterned glass by applying voltage between electrode pad 1 to pad 2–6, as marked in the photos, respectively. Adapted with permission from ref. [120]. Copyright 2017, Royal Society of Chemistry.

fabrication. To reduce fabrication cost and improve yield, the patterned surface was further used as a recyclable template for delivering liquid droplet matrix onto various substrate surfaces, as schematically shown in Fig. 17a. The liquid droplet matrix was formed on the Au structures patterned on the Si stamp, by immersing into and pulling out from the solution. When brought to contact with the sample surface, the droplets are partially transferred after removal of the stamp. The amount of the liquid droplets to be transferred is determined by adhesion force which depends on surface tension, contact angle and contact radius of the liquid on the both surfaces. Notably, the stamp can be recycled for over 100 times without obvious contamination [123].

The liquid droplet transfer printing also enables multi-species patterning to define various materials with different functions on a single surface, as shown in fluorescence microscope images in Fig. 17b-d. Initially, the red rhodamine 6 G-dyed glycerol droplet array on the stamp plate was transfer printed onto an ITO-covered glass, exhibiting red dot emitting array (Fig. 17b). The stamp was then changed to green fluorescein-doped glycerol droplet array, by keeping the ITO-covered glass fixed on the sample holder. Using a manual micropositioning stage and angle adjuster analogous to alignment in photolithography, the fluorescein-doped glycerol liquid droplet array was printed successfully onto the sample plate, demonstrating a red–green bi-color pattern (Fig. 17c). By repeating the procedure, a 7-hydroxycoumarin-doped glycerol droplet array was printed, forming a red-green-blue tri-color pattern (Fig. 17c) [124].

4.3. Templated pattering of functional materials in emulsion

Emulsions are mixture of two immiscible liquids, with one being dispersed in another by mechanical agitation and in presence of

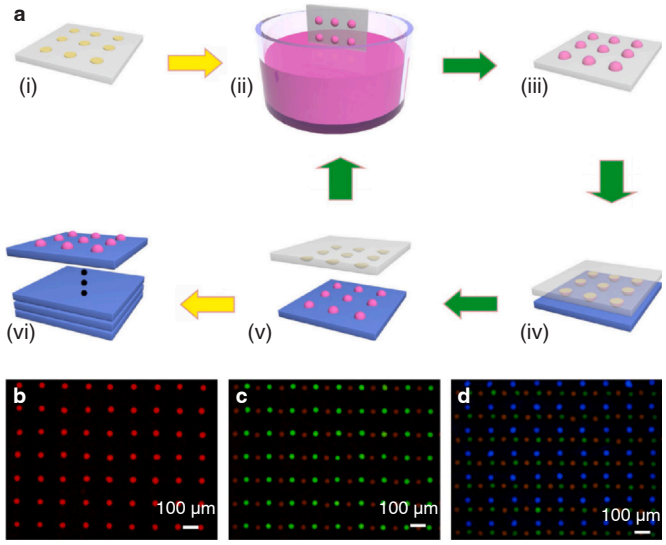

Fig. 17. a) The schematic illustration of the liquid droplet matrix transfer printing process: (i) Au patterned Si stamp, (ii) immersing the stamp into the solution, (iii) formation of micro-liquid droplet array after withdrawing the stamp, (iv) transfer printing of the liquid droplets on the sample surface, (v) removing the stamp for recycling, and (vi) duplication of the liquid droplet arrays. Adapted with permission from ref. [123]. Copyright 2017, Royal Society of Chemistry. Fluorescence microscope images of b) rhodamine 6G, c) fluorescein, and d) 7-hydroxycoumarin dyed glycerol printed on ITO-covered glass. Adapted with permission from ref. [124]. Copyright 2019, American Institute of Physics.

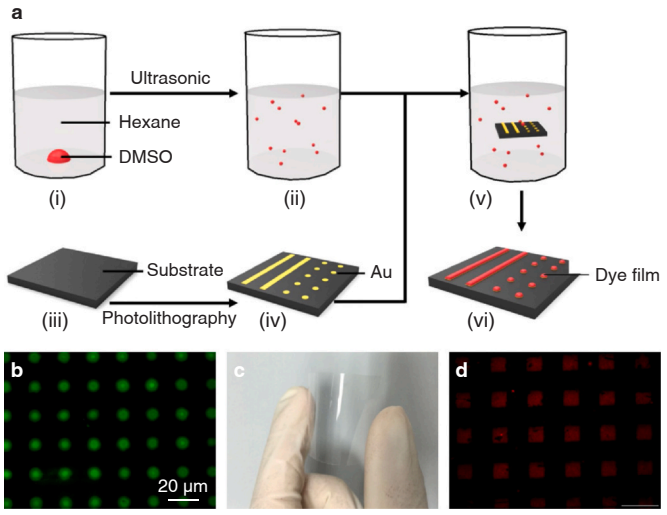

Fig. 18. a) Schematic representation of template patterning of functional organic materials in emulsion: i) mixture of two immiscible liquids, ii) ultrasonic treatment of the mixture to form emulsion, iii) OTS modification of SiO_2, iv) patterning of substrate by standard photolithography, v) immersion of the templates into the emulsions, and vi) formation of patterned dye films after evaporation of solvent. b) Fluorescence microscope image of Alq3 on 4 μm Au dot array patterned OTS/Si. c) Photography and d) fluorescence microscope images of Rhodamine 6 G on 20 μm Au square array patterned PET substrate. Adapted with permission from ref. [126]. Copyright 2016, Wiley-VCH Verlag GmbH.

surfactants. Typically emulsions contain thermodynamically unstable droplets in size of micro/nanometers, exhibiting classic Brownian motion in the continuous phase [125]. The lifetime of an emulsion depends on system composition and the way of processing, varying from minutes to years through destruction mechanisms of Ostwald ripening and coalescence. The motion and destruction of emulsion droplets provide an opportunity for selective absorption onto hydrophilic patterned surfaces. Experimentally a small portion of dyed dimethyl sulfoxide (DMSO) was added to hexane, and then emulsion was created by agitating the mixture with ultrasonic. Then Au patterned Octadecyltrichlorosilane (OTS) modified SiO_2 templates, which were prepared by standard photolithography, were immersed into the DMSO/hexane emulsion for several minutes to allow the dyed DMSO droplets selectively absorbed onto the Au. Finally, the samples were taken out the mixture to form patterned dye films on the Au by evaporation of solvent, as schematically shown in Fig. 18a.

Owing to the spatial confinement of the droplets, the strategy enables to fabricate various functional organic material patterns with different shapes on substrates of interests, as shown in Fig. 18b-d. For instance, aluminium-tris(8-hydroxychinolin), a green light emissive molecule widely used as an electron transport layer in OLEDs, was successfully patterned on 4 μm Au dot array with the procedure, as shown in fluorescence microscope image of Fig. 18b. Importantly, the technique can easily be extended to arbitrary patterns on substrates of interest over large area, as demonstrated with Rhodamine 6 G on 20 μm Au square array on flexible polyethylene terephthalate (PET) substrate in Fig. 18c-d [126].

4.4. Area selective nucleation of molecules by micro-spacing in air sublimation

Recently, a novel technique called micro-spacing in-air sublimation has been developed for the growth of high quality organic semiconductor crystals [127]. In this method, the source and substrate

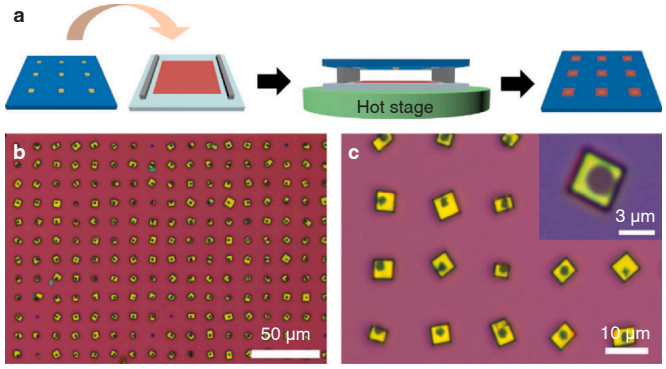

Fig. 19. a) Schematic procedure steps to fabricate organic single crystal array by micro-spacing in-air sublimation. Left: Au dot array patterned substrate was positioned on a Si wafer with organic semiconductor powder, where two glass spacers were used to separate the patterned surface and Si wafer; middle: heating the Si wafer with a hot stage; right: remove the sample from the spacers and then an organic single crystal array was obtained. b) Large area and (c) high resolution optical microscope images of perylene pattern on Au array with periodicity of 15 μm. The inset in (c) shows the high-resolution image of a single perylene crystal located on an Au dot. Adapted with permission from ref. [128]. Copyright 2022, Wiley-VCH Verlag GmbH.

surface is spaced at a very small distance, comparable to the mean free path of evaporated molecules, typically in the range of hundreds of micrometers. Systematic investigations have revealed that deposited molecules first form droplets on the substrate surface, and subsequently, organic semiconductor single crystals separate out from these droplets, avoiding the formation of grain boundaries commonly observed in conventional vacuum deposition.

Fig. 19a illustrates the schematic procedure to grow organic semiconductor single crystal arrays by micro-spacing in-air sublimation. Firstly, Au patterns were fabricated as the nucleation centers for molecules, through standard lithography on SiO_2 surface. Then, organic semiconductor powders were evenly coated on a silicon wafer, serving as organic evaporation source. Two glass spacers were placed on the two sides of this Si wafer to maintain a small separation between source and sample surface. Subsequently, the sample was placed on the glass spacers with the Au pattern facing to the organic source. Upon heating the organic source, the organic semiconductor molecules were sublimated to the patterned substrate and selectively grown on the Au pattern. Organic single crystal array was obtained by removing the sample from the spacers.

The selective nucleation of molecules on Au pattern by micro-spacing in-air sublimation was proved using a planar molecule perylene. The Au pattern consists of a dot array with the diameter of 2 μm, periodicity of 15 μm. The source and sample are separated by a glass spacer in thickness of 200 μm. Optical microscope image (Fig. 19b) shows almost all organic semiconductor crystals locate on Au dots, and no extra one was found on SiO_2 area. High-resolution optical images in Fig. 19c revealed that the perylene crystals have a quadrilateral shape, a typical feature of single crystal. The crystallinity of crystals was further confirmed by selected-area electron diffraction (SAED) showing sharp and discrete diffraction spots in the diffraction patterns [128].

5. Ultra-high resolution microelectronic and optoelectronic devices

Analog to their inorganic counterparts, organic semiconductors have be employed in various microelectronic and optoelectronic devices since 1980 s. Key achievements in material synthesis, precise control over thin film deposition, creation of p-n junction, carrier

doping, and contact resistance engineering have paved the way for high performance devices, including OLEDs, OFETs, organic solar cells, photo-detectors and memories. Most of these devices require precise patterning for their applications. Notably, wearable electronics, such as near-eye-displays demand an ultra-high resolution up to 4 K ppi for immersive experiences. Nowadays, the organic device pattering in ultra-high resolution, with high yield over large area, is still a big challenge. The versatility of patterned growth strategy could provide a promising way to realize a lithography compatible technique for patterning organic device in ultra-high resolution.

5.1. Organic light emitting diodes (OLEDs)

When biased under certain electrical fields, organic p-n junctions emit light through the recombination of electrons and holes that injected from cathode and anode, respectively [18]. The intrinsic properties of an OLED, such as emitting wavelength and efficiency, are significantly influenced by the materials used, device structures and their processing procedures employed [129]. OLEDs are widely commercialized in various applications, particularly in middle and small size displays with typical resolution ranging from 300 to 1000 ppi.

To demonstrate the feasibility of patterned growth in fabricating high resolution OLEDs, area selective growth of NPB on Au dots patterned indium tin oxide (ITO) glass was employed as the hole injection and transport layer. Subsequently, with the deposition of electron injection and transport layer of Alq3, and the cathode layer of Al, a classic bi-layer OLED structure was formed, as schematically shown in Fig. 20a. When the p-n junction of NPB/Alq3 is positively biased, the electrons and holes are injected into the corresponding layers from anode and cathode electrodes, respectively. The carriers then diffuse to p-n junction, forming excitons which further recombine to emit photons (light). The resolution of the micro-OLEDs is entirely determined by the template that can be processed by the techniques for inorganics.

In case of an Au dot array with 0.5 μm in diameter and 1 μm in periodicity, OLEDs in resolution as high as 25 K ppi was achieved (Fig. 20b) [130]. The technique can be readily extended to create RGB micro-OLEDs with arbitrary shapes. For example, electron-luminescent patterns of “OLED” in red, green and blue colors were achieved using emission systems of the red of ITO-Au/NPB(20 nm)/Alq3:DCM (35 nm:1 %)/Alq3 (35 nm)/Al, the green of ITO-Au/NPB(20 nm)/Alq3(70 nm)/Al and the blue of ITO-Au/NPB (20 nm)/PPIPPI-TPA(30 nm)/TPBI (50 nm)/Al, respectively (Fig. 20c). Using flexible substrates such as PEN, flexible micro-OLEDs are further obtained with NPB/Alq3 bi-layer structure, as shown in Fig. 20d [131]. The device performance can further be enhanced using conducting polymer polypyrrole (PPy) as nucleation layer for the molecules, owing to the excellent transparency of PPy for light extraction [132].

5.2. Organic field effect transistors (OFETs)

An OFET is a three terminal device that allows control of source-drain current by a third gate electrode. Benefiting from the advancements in material design and crystalline growth, the carrier mobility in organic semiconductors has reached up to 40 cm^2/V.s [20], substantially surpassing that of amorphous silicon. Although high quality organic micro-crystals are easily obtained on substrate surface either by vacuum deposition or solution processing, their random distribution in size and location make them difficult to be addressed in applications such as driving active matrix display. Hence, for the high integration level applications, fabrication of uniform single crystals and their addressing by reading-out electrodes remains underdeveloped.

In case of step-edge induced area selective growth, the PTCDI-C8 films selectively grow between the Au stripes patterned on SiO_2

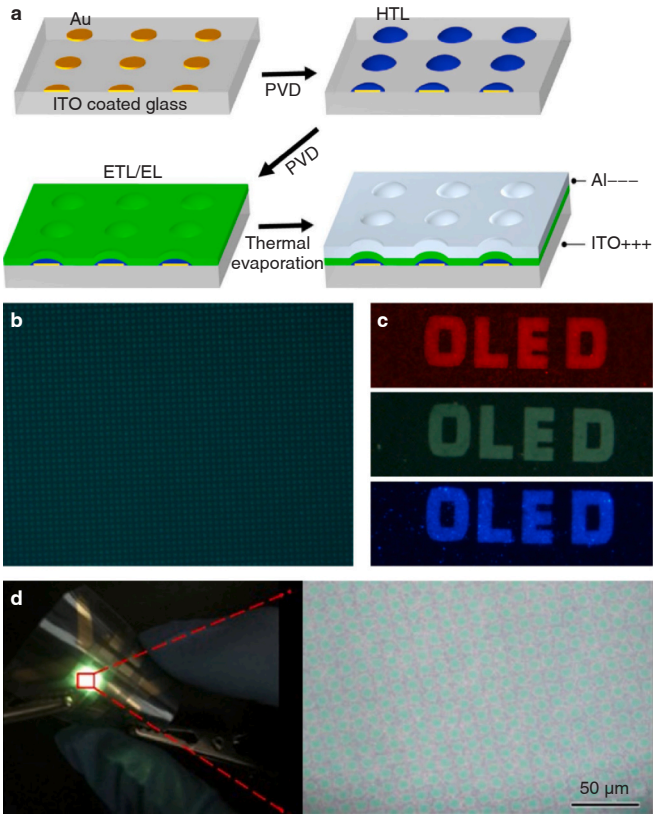

Fig. 20. a) Schematic diagram of the fabrication procedure for Micro-OLEDs: i) Au patterned ITO glass as the anode electrode, ii) selective growth of hole-transporting layer on patterned surface, iii) subsequently upon deposition of electron-transporting/emitting layer, and v) Al layer as the cathode electrode. b) Green luminescence image of the OLED array with a diameter of 0.5 μm and a periodicity of 1 μm. c) Red, green and blue luminescence image of the text ‘OLED’ with a line width of 20 μm. Adapted with permission from ref. [130]. Copyright 2017, Royal Society of Chemistry. d) The photo of the flexible OLED device under operation (left) and the high-magnification microscope image of electroluminescent area (right). Adapted with permission from ref. [131]. Copyright 2020, Wiley-VCH Verlag GmbH.

(Fig. 6b). The structures were further configured as OFET devices by taking the Au stripes as source/drain electrodes, the SiO_2 as dielectric layer, and patterned PTCDI-C8 as active layer, with an electron mobility up to 1 cm^2/V.s [84]. With PTCDA nano crystals selectively nucleated on Au lines, bridging source and drain electrodes with organic crystalline nanowires were also achieved by seeded growth of NPB, leading to a hole mobility in the order of 10^{-3} cm^2/V.s [133]. However, the electrical characterization of devices fabricated by the two methods revealed a very low yield, indicating poor contacts at the Au and organic interfaces. The poor contact might result from the thermal contraction of organic films when cooled to room temperature after deposition at elevated substrate temperature.

To achieve high-resolution single crystalline OFET array with a high yield, an approach combing binding energy difference induced area selective growth and solvent vapor annealing (SVA) was developed. In this method, organic semiconductors were vacuum deposited onto SiO_2 surface patterned with Au electrodes, forming amorphous molecular domains precisely located on closed spaced electrode pairs. These amorphous molecular domains were then transformed into single micro-crystals by exposure to saturated organic solvent vapor, resulting in OFET arrays by taking the SiO_2 as dielectric layer, as schematically shown in Fig. 21a. Experimentally the semiconducting molecule of

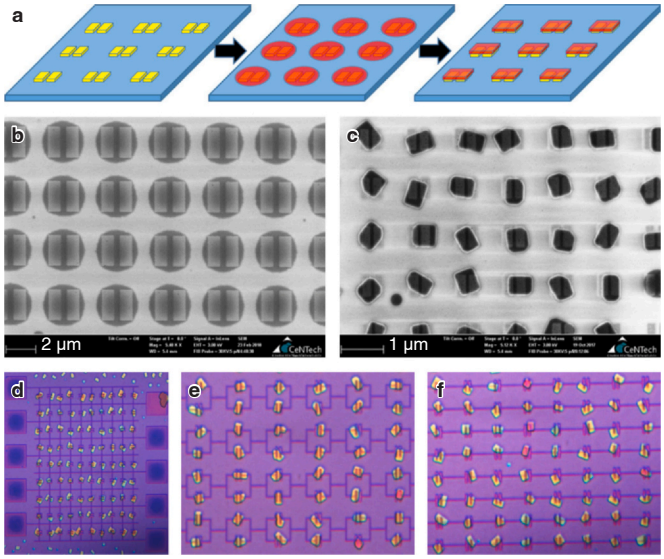

Fig. 21. a) Schematic procedure of fabricating organic crystalline array combing area selective growth and solvent vapor annealing. Left: patterning Au electrode pairs on SiO_2; middle: selective growth of TESADT molecules on electrode pairs; right: formation of single-crystal array by SVA. Scanning electron microscopy (SEM) images of TESADT b) selectively grown on Au electrode pairs and c) subsequently treated via SVA on Au array with periodicity of 1.5 μm. Optical microscope images of d) 9 × 10 OFET array with addressing electrode pads, and basic logic gates of e) AND and f) OR arrays. Adapted with permission from ref. [135]. Copyright 2020, American Chemical Society.

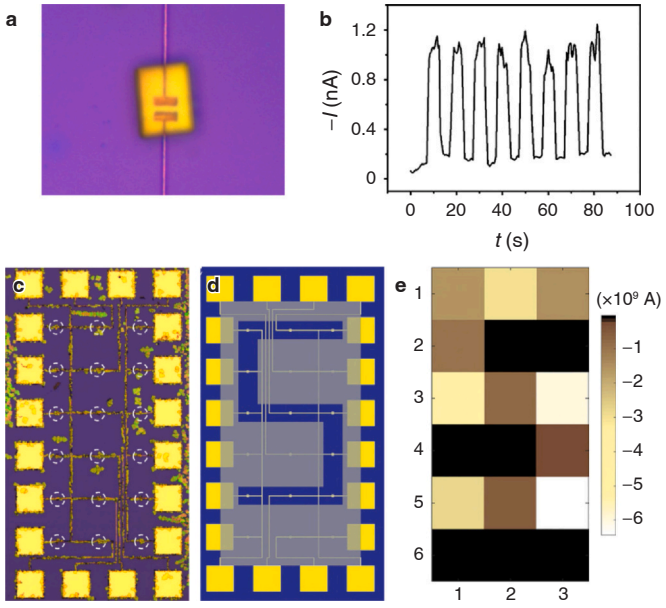

Fig. 22. a) Optical microscope image of a perylene single crystal bridges source–drain electrodes, where the channel width and channel length are 5 and 1 μm, respectively. b) Time-resolved photo response curve at a bias voltage of −40 V with the light source switched on/off every 5 s. c) Optical microscope image of a 3×6 array of addressable photodetector circuit, where each device is marked by white dashed circles. d) Schematic diagram of the mask with pattern of letter "S" placed on the photodetector circuit. e) A diagram of measured currents expressing the output response of the circuit, where the X-axis, Y-axis and Z-axis represent the abscissa, ordinate and current value of each device in the array. Adapted with permission from ref. [128]. Copyright 2022, Wiley-VCH Verlag GmbH.

triethylsilylethynyl anthradithiophene (TES-ADT) was used as an example [134]. The TES-ADT contains triisopropylsilylethynyl group to provide a high solubility of the molecule in organic solvents, and also endows the anthradithiophene part to form compact molecular packing with reduced intermolecular distance in π−π stacking. With 12 nm TES-ADT deposited on Au pair array in spacing of 1.5 μm, the SEM image reveals that every Au electrode pair is occupied by one TES-ADT island in uniform size (Fig. 21b). Together with the diffraction peaks observed in the XRD measurements, the liquid droplet-like morphology indicates that the TESADT islands could consist of very tiny nanocrystals embodied in amorphous surrounding. Upon exposure to solvent vapor, the droplet-like islands of TES-ADT exhibited a volume expansion initially by absorbing the solvent, and then gradually evolved to quadrilateral shaped micro-plates, indicating the formation of microcrystals (Fig. 21c).

Benefited from the positioned growth, the fabricated single-crystalline micro-plates can be readily addressed by pre-patterned Au electrodes, directly leading to single-crystal OFET arrays utilizing the SiO_2 as insulating gates. The average hole mobility extracted from the transfer curves is calculated to be 0.056 cm^2/V.s, representing a two-order improvement compared to as-grown samples. Cross-talk, which defined as interference between neighboring operating devices, can be completely suppressed due to the isolation of the discrete microcrystals. The "first position, then crystallization" strategy further allows the microcrystals not only to be positioned at designated locations, but also readily addressed by connecting lines. Fig. 21d-f show microscope images of an OFET array containing 9 × 10 pixels with reading-out Au pads surrounding, and two logic units containing 6 × 4 pixels of OR and 4 × 8 pixels of AND logic gate arrays, respectively [135]. Consequently, the strategy provides the flexibility to design the circuits by utilizing a bottom-gate bottom electrode configuration.

5.3. Organic photodectors (PDs)

Photodetectors are devices that convert light into electrical signals, in device configuration with either two or three terminals. For applications like image sensing and intelligent gesture recognition, addressable and cross-talk free organic photodetector arrays in high resolution are urgently demanded for more accurate sensing. Microcrystals fabricated by micro-spacing in-air sublimation or solvent vapor annealing can further be employed for photdetector array fabrication, which could directly addressed by reading out circuit. Fig. 22a shows a typical optical microscope image of microsized perylene single crystal, bridging an electrode pair which connected to electrical characterization instruments. The devices exhibited an ultralow dark current in order of 10^{-11} A, indicating a high quality of the crystals. An on/off ratio above 70 was obtained by irradiating the devices under 45 mW/cm^2. Time resolved photo-response (Fig. 22b), by measuring the photocurrent with the irradiation light switched on and off every 5 seconds, shows the stability of devices with response time in about 1 second. Benefiting from the positioned growth of micro-crystals, an organic photodetector matric containing 3×6 single crystal photodetectors was fabricated. With the method, large area arrays with device size scaled down to micrometers can be achieved. For instance, figure 23c shows an array with a device size of 6×10 $μm^2$ marked in the white dashed circles. With optimized deposition amount, no physical contact of organic crystals with adjacent devices can be controlled, resulting in crosstalk free photodetector array. When the matrix covered by a mask patterned with letter "S" (schematically shown in Fig. 22d), a spatial mapping of the letter was presented by scanning the

photocurrent of each device under illumination (Fig. 22e) [128]. In principle, the method could be extended for multispecies patterning to precisely position materials with different photo-responses on a single substrate, achieving full-spectrum detection in high spatial resolution.

6. Conclusions and outlook

To date, research on organic semiconductor has made tremendous progress since the emergence of thin film OLEDs, OFETs and OPVs in last three decades. Commercial products based on organic semiconductors, such as wearable health monitoring and near-eye displays, have become integral parts of our daily lives. However, these devices are primarily processed using fine metal mask technology in consideration to reliability and cost, which results in a typical resolution of under 1 K ppi [136]. The development of AR/VR put an ever-increasing demand for high display resolution to avoid screen door effect and achieve an immersive experience. Currently, ultra-high resolution micro-OLED displays are mainly realized by filtering white light with red, green and blue filters, respectively [137]. The approach leads to high power consumption and low device efficiency, which in return deteriorate the device lifetime.

With the concept of “surface patterning and patterned growth”, three selective growth mechanisms are observed: namely induced by surface molecular density modulation, difference in binding energy and step-edges. Both experimental results and theoretical simulation revealed that the mechanism is determined by the interactions of molecule with template, substrate and molecule itself. With binding energy difference and step-edges induced area selective growth mechanisms, the molecules can be completely controlled to grow on the designated locations, resulting in a 100 % pattern formation. However, owing the fluctuation of molecule density on surface, only 95 % of pattern yield was achieved by surface molecular density modulation. The patterned structures can further dimensionally and physically engineered for diverse applications. Besides patterning small molecule in vacuum, the strategy can be extended to in air, solution and emulsion systems to structure various functional materials such as polymers and quantum dots. Last but not least, various device arrays with resolution of up to 25 K ppi were achieved, catering the requirements for the most applications in organic electronics. The procedure is completely compatible to the conventional Si processing technologies, including photolithography. We believe the methods represent essential steps toward practical applications of organic semiconductor devices in ultra-high resolutions. However, considerable work is still required to turn the patterned growth technique into a truly viable technology.

6.1. *In situ and real time characterization of growth dynamics*

As an emerging research field, the patterned growth is still under development in many aspects. For instance, although the selective growth mechanisms and wetting behaviors were physically addressed, a complete understanding of the growth dynamics is not confirmed. The challenge partly lies on the absence of techniques to characterize the growth process, owing to sensitivity of organic materials to the environment. Currently the *ex situ* and separated characterizations on samples might lead to inconsistencies in temporal, spatial and structural evolution, due to post annealing effect and impurity absorption when exposing the samples to atmosphere, or uniformity fluctuation during deposition [138,139]. Single mode *in situ* characterization was also employed to monitor the morphological and electrical evolution during patterned growth with a certain success [140–144]. Ideally, a multimode *in situ* characterization on a same micro-spot, allowing the optical, electrical, morphological, structural and spectral properties to be measured at same time, could provide comprehensive and precise information to exclude the inconsistency and deviation, thus contribute to the further developments of the patterned growth.

6.2. *Theoretical modeling of the system*

Numerical simulations using modified Monte Carlo (MC) methods were performed to replicate the growth process of molecules on patterned surfaces, including beam generation, surface diffusion, nucleation on designated locations and desorption from surfaces [93,145]. In the simulations, the material system comprising substrate, template and organic semiconductors were modeled as spheres that designated to different interaction. Employing simple Lennard-Jones pair potentials, the simulation outcomes closely matched the molecular behaviors in experiments which mainly involves diffusion and nucleation, such as binding energy difference and surface molecular density modulation induced patterned growth. Interpretation of step-edge induced area selective growth and orientation control, anisotropic wetting and molecular phase separation were attempted by several groups, based on the modified MC methods [94,146]. However, the MC methods with molecules modeled as spheres are over simplified, neglecting anisotropic interaction and collective motion of molecules during the process. Therefore, advanced models capable of representing specific interaction between molecules, such as π-π overlapping and collective motion, are required for more accurate simulation of the systems, yielding convincing results.

6.3. *Monolithic integration of microelectronics with optoelectronics*

The integration of various semiconductor devices on a single chip plays a crucial role in the practical applications. For instance, sensors perform signal collections, microelectronics provide signal transmission and processing, and optoelectronics function in signal displaying [147]. As a whole, the integration realizes a system for specific functions. For this perspective, monolithic integration should not be limited to organic semiconductor materials alone, but rather extended to all material systems, e.g., to fully explore the added value of well-established CMOS platform to organic semiconductor [148]. The patterned growth of organic semiconductors on Si substrate provides an opportunity for integration of high performance Si CMOS to driven OLED arrays. To date, various ultra-resolution organic semiconducting device arrays are successfully demonstrated with the patterned growth strategy. However, the practical applications will further requires fully integration of multi-devices, such as direct construction of OLEDs on TFT arrays.

6.4. *Full color integration of OLEDs*

Combining OLEDs with multiple emissions on a single substrate also is of significant importance in a number of applications, such as forming the red, green and blue emitting pixels of full-color displays. With the patterned growth, single-color red, green and blue OLED arrays with pixel resolution up to 25 K ppi have been achieved [130]. Single color displays may find some applications for displaying information, notifications, or simple graphics. However , high resolution full color micro-displays are still an urgently demanded to keep up with the pace of fast developments in near-eye displaying [149,150]. In principle, the emission wavelength of an OLED is determined by the recombination region of excitons driven by external fields. A control over carrier diffusion before the exciton formation could open up a way for the multicolor integration, e.g., using heteropatternng achieved by patterned growth to control the traveling length of carriers, and thus leading to the recombination of excitons in different regions.

6.5. Device performance and their applications in wearable electronics

The ultra-high resolution OLED, OFET and OPD device arrays were successfully fabrication with the patterned growth strategy. However, the devices demonstrated relatively low performance to those fabricated by top-down strategies. The low device performance originated partly from the device configuration, e.g., the bottom-gate bottom-electrode OFET and simple bi-layer OLED structure. Additionally, the Au electrodes were not modified to match the energy level of organic semiconductors, which leads to unfavorable carrier injection and degrade device performance. We expect an improved device performance by optimization of device configuration, as well as electrode modification. For the applications in wearable electronics, the devices would typically withstand a certain strain during operation. Although all the three selective nucleation mechanisms have been successfully applied in high resolution organic semiconductor device patterning on flexible substrates [131], further testing of the devices in operando modes, e.g. under strain states, is still required to valid the success of the technique.

In the pursuit of developing a lithographically compatible device processing platform for organic semiconductors, patterned growth has been validated as a versatile method for efficiently generating high-resolution patterns over large areas. While significant progress has been made in laboratory settings with small samples, considerable work is still needed to enable the technique's implementation in mass production, especially when scaling up to larger sample sizes. Challenges related to yield, uniformity, and cost must be addressed. With ongoing efforts dedicated to these areas, we anticipate that this strategy will open new opportunities for ultra-high-resolution organic semiconductor devices.

CRediT authorship contribution statement

Wenchong Wang: Conceptualization, Investigation, Projection administration, Supervision, Writing-Original Draft. **Lifeng Chi:** Conceptualization, Investigation, Projection administration, Supervision, Funding acquisition, Writing-Review & Editing.

Declaration of Competing Interest

The authors declare that they have no known competing financial interests or personal relationships that could have appeared to influence the work reported in this paper.

Acknowledgements

The authors acknowledge financial support from the National Natural Science Foundation of China (Grant Nos. 51821002), the Suzhou Key Laboratory of Surface and Interface Intelligent Matter (Grant SZS2022011) and the Gusu Innovation and Entrepreneurship Talent Program-Major Innovation Team (ZXD2023002). This work is also supported by the Collaborative Innovation Center of Suzhou Nano Science & Technology, the Priority Academic Program Development of Jiangsu Higher Education Institutions (PAPD), and the 111 Project.

References

[1] S.R. Forrest, The path to ubiquitous and low-cost organic electronic appliances on plastic, Nature 428 (2004) 911–918.
[2] C.L. Wang, H.L. Dong, W.P. Hu, Y.Q. Liu, D.B. Zhu, Semiconducting π-conjugated systems in field-effect transistors: a material odyssey of organic electronics, Chem. Rev. 112 (2012) 2208–2267.
[3] A. Mishra, P. Bäuerle, Small molecule organic semiconductors on the move: promises for future solar energy technology, Angew. Chem. Int. Ed. 51 (2012) 2020–2067.
[4] S.P. Wang, X.J. Yan, Z. Cheng, H.Y. Zhang, Y. Liu, Y. Wang, Highly efficient near-infrared delayed fluorescence organic light emitting diodes using a phenanthrene-based charge-transfer compound, Angew. Chem. Int. Ed. 54 (2015) 13068–13072.
[5] K. Yoshida, J. Gong, A.L. Kanibolotsky, et al., Electrically driven organic laser using integrated OLED pumping, Nature 621 (2023) 746–752.
[6] W. Jiang, Y. Lia, Z.H. Wang, Heteroarenes as high performance organic semiconductors, Chem. Soc. Rev. 42 (2013) 6113–6127.
[7] D.P. Hagberg, J.H. Yum, H. Lee, F. De Angelis, T. Marinado, K.M. Karlsson, R. Humphry-Baker, L.C. Sun, A. Hagfeldt, M. Gratzel, M.K. Nazeeruddin, Molecular engineering of organic sensitizers for dye-sensitized solar cell applications, J. Am. Chem. Soc. 130 (2008) 6259–6266.
[8] T. Baumgartner, Insights on the design and electron-acceptor properties of conjugated organophosphorus materials, Acc. Chem. Res. 47 (2014) 1613–1622.
[9] W.G. Zhu, R.H. Zheng, Y.G. Zhen, Z.Y. Yu, H.L. Dong, H.B. Fu, Q. Shi, W.P. Hu, Rational design of charge-transfer interactions in halogen-bonded co-crystals toward versatile solid-state optoelectronics, J. Am. Chem. Soc. 137 (2015) 11038–11046.
[10] Z.T. Liu, G.X. Zhang, D.Q. Zhang, Modification of side chains of conjugated molecules and polymers for charge mobility enhancement and sensing functionality, Acc. Chem. Res. 51 (2018) 1422–1432.
[11] E.H. Suh, S.B. Kim, J. Jung, J. Jang, Extremely electron-withdrawing Lewis-paired CN groups for organic p-dopants, Angew. Chem. Int. Ed. 135 (2023) e202304245.
[12] M. Planells, A. Abate, D.J. Hollman, S.D. Stranks, V. Bharti, J. Gaur, D. Mohanty, S. Chand, H.J. Snaith, N. Robertson, Diacetylene bridged triphenylamines as hole transport materials for solid state dye sensitized solar cells, J. Mater. Chem. A 1 (2013) 6949–6960.
[13] Y. Diao, B.C. Tee, G. Giri, J. Xu, D.H. Kim, H.A. Becerril, R.M. Stoltenberg, T.H. Lee, G. Xue, S.C. Mannsfeld, Z.N. Bao, Solution coating of large-area organic semiconductor thin films with aligned single-crystalline domains, Nat. mater. 12 (2013) 665–671.
[14] Z.W. Wang, S.G. Wang, L.Z. Huang, L.Q. Li, L.F. Chi, L, Microstructured ultrathin organic semiconductor film via dip-coating: precise assembly and diverse applications, Acc. Mater. Res. 1 (2020) 201–212.
[15] J.L. Yang, D.H. Yan, Weak epitaxy growth of organic semiconductor thin films, Chem. Soc. Rev. 38 (2009) 2634–2645.
[16] C.W. Tang, S.A. VanSlyke, Organic electroluminescent diodes, Appl. Phys. Lett. 51 (1987) 913–915.
[17] A. Tsumura, H. Koezuka, T. Ando, Macromolecular electronic device: Field-effect transistor with a polythiophene thin film, Appl. Phys. Lett. 49 (1986) 1210–1212.
[18] C.W. Tang, Two-layer organic photovoltaic cell, Appl. Phys. Lett. 48 (1986) 183–185.
[19] H. Sirringhaus, H., Organic field-effect transistors: the path beyond amorphous silicon, Adv. Mater. 26 (2014) 1319–1335.
[20] H. Minemawari, T. Yamada, H. Matsui, J.Y. Tsutsumi, S. Haas, R. Chiba, R. Kumaiand, T. Hasegawa, Inkjet printing of single-crystal films, Nature 475 (2011) 364–367.
[21] H.B. Wang, D.H. Yan, Organic heterostructures in organic field-effect transistors, NPG Asia Mater. 2 (2010) 69–78.
[22] C. Gao, A. Shukla, H.K. Gao, Z.G. Miao, Y.H. Zhang, P. Wang, G.W. Luo, Y. Zeng, W.W.H. Wong, T.A. Smith, S.C. Lo, W.P. Hu, E.B. Namdas, H.L. Dong, Harvesting triplet excitons in high mobility emissive organic semiconductor for efficiency enhancement of light-emitting transistors, Adv. Mater. 35 (2023) 2208389.
[23] C.D. Müller, A. Falcou, N. Reckefuss, M. Rojahn, V. Wiederhirn, P. Rudati, H. Frohne, O. Nuyken, H. Becker, K. Meerholz, Multi-colour organic light-emitting displays by solution processing, Nature 421 (2003) 829–833.
[24] K.H. Kim, J.J. Kim, Origin and control of orientation of phosphorescent and TADF dyes for high-efficiency OLEDs, Adv. Mater. 30 (2018) 1705600.
[25] X. Ai, E.W. Evans, S.Z. Dong, A.J. Gillett, H.Q. Guo, Y.X. Chen, T.J.H. Hele, R.H. Friend, F. Li, Efficient radical-based light-emitting diodes with doublet emission, Nature 563 (2018) 536–540.
[26] J. Bertrandie, J.H. Han, C.S.P. De Castro, E. Yengel, J. Gorenflot, T. Anthopoulos, F. Laquai, A. Sharma, D. Baran, The energy level conundrum of organic semiconductors in solar cells, Adv. Mater. 34 (2022) 2202575.
[27] Z.B. Henson, K. Müllen, G.C. Bazan, Design strategies for organic semiconductors beyond the molecular formula, Nat. Chem. 4 (2012) 699–704.
[28] M.D. Allendorf, R.H. Dong, X.L. Feng, K. Kaskel, D. Matoga, V. Stavila, Electronic devices using open framework materials, Chem. Rev. 120 (2020) 8581–8640.
[29] Z. Wang, J. Hu, J. Lu, X.F. Zhu, X. Zhou, L.Z. Huang, L.F. Chi, Charge transport manipulation via interface doping: achieving ultrasensitive organic semiconductor gas sensors, ACS Appl. Mater. Interfaces 15 (2023) 8355–8366.
[30] M. Schwarze, W. Tress, B. Beyer, F. Gao, R. Scholz, C. Poelking, K. Ortstein, A.A. Günther, D. Kasemann, D. Andrienko, K. Leo, Band structure engineering in organic semiconductors, Science 352 (2016) 1446–1449.
[31] C. Tanase, E.J. Meijer, P.W.M. Blom, D.M. De Leeuw, Unification of the hole transport in polymeric field-effect transistors and light-emitting diodes, Phys. Rev. Lett. 91 (2003) 216601.
[32] S.J. Wang, M. Sawatzki, G. Darbandy, F. Talnack, J. Vahland, M. Malfois, A. Kloes, S. Mannsfeld, H. Kleemann, K. Leo, Organic bipolar transistors, Nature 606 (2022) 700–705.
[33] W. Brütting, Introduction to the physics of organic semiconductors, Phys. Org. Semicond. (2005) 1–14.

[34] M. Kaltenbrunner, T. Sekitani, J. Reeder, T. Yokota, K. Kuribara, T. Tokuhara, M. Drack, R. Schwödiauer, I. Graz, S. Bauer-Gogonea, S. Bauer, T. Someya, An ultra-lightweight design for imperceptible plastic electronics, Nature 499 (2013) 458–463.
[35] M. Moser, A. Wadsworth, N. Gasparini, I. McCulloch, Challenges to the success of commercial organic photovoltaic products, Adv. Energy Mater. 11 (2021) 2100056.
[36] X.R. Zhang, H.T. Deng, X. Zeng, Y.L. Wang, P. Huang, X.S. Zhang, Recent progress of patterned electrodes in wearable electronics: fabrication and application, J. Phys. D: Appl. Phys. 57 (2023) 013001.
[37] K. Yan, J.A. Li, L.J. Pan, Y. Shi, Inkjet printing for flexible and wearable electronics, APL Mater. 8 (2020) 120705.
[38] C. Wang, X.T. Zhang, H.L. Dong, X.D. Chen, W.P. Hu, Challenges and emerging opportunities in high-mobility and low-energy-consumption organic field-effect transistors, Adv. Energy Mater. 10 (2020) 2000955.
[39] S. Oren, H. Ceylan, P.S. Schnable, L. Dong, High-resolution patterning and transferring of graphene-based nanomaterials onto tape toward roll-to-roll production of tape-based wearable sensors, Adv. Mater. Techno. 2 (2017) 1700223.
[40] K. Bagchi, M.D. Ediger, Controlling structure and properties of vapor-deposited glasses of organic semiconductors: recent advances and challenges, J. Phys. Chem. Lett. 11 (2005) 6935–6945.
[41] S.N. Cheng, Y.J. Lee, J.G. Yu, L. Yu, M.D. Ediger, Surface equilibration mechanism controls the stability of a model codeposited glass mixture of organic semiconductors, J. Phys. Chem. Lett. 14 (2023) 4297–4303.
[42] Z.Z. Luo, X.X. Song, X.L. Liu, X.G. Lu, Y. Yao, J.P. Zeng, Y.T. Li, D.W. He, H.J. Zhao, L. Gao, Z.H. Yu, W. Niu, H.B. Sun, Y. Xu, S.J. Liu, W. Qin, Q. Zhao, Revealing the key role of molecular packing on interface spin polarization at two-dimensional limit in spintronic devices, Sci. Adv. 9 (2023) eade9126.
[43] S. Verlaak, S. Steudel, P. Heremans, D. Janssen, M.S. Deleuze, Nucleation of organic semiconductors on inert substrates, Phys. Rev. B 68 (2003) 195409.
[44] B. Stadlober, U. Haas, H. Maresch, A. Haase, Growth model of pentacene on inorganic and organic dielectrics based on scaling and rate-equation theory, Phys. Rev. B 74 (2006) 165302.
[45] J.J. De Yoreo, P.G. Vekilov, Principles of crystal nucleation and growth, Rev. Mineral. Geochem. 54 (2003) 57–93.
[46] T. Sekiya, T. Sasaki, K. Hane, Design, fabrication, and optical characteristics of freestanding GaN waveguides on silicon substrate, J. Vac. Sci. Technol. B 33 (2015) 031207.
[47] Y.Y. Xu, F. Zhang, X.L. Feng, Patterning of conjugated polymers for organic optoelectronic devices, Small 7 (2011) 1338–1360.
[48] R.Z. Chen, X.J. Wang, X. Li, H.X. Wang, M.Q. He, L.F. Yang, Q.Y. Guo, S. Zhang, Y. Zhao, Y. Li, Y.Q. Liu, D.C. Wei, A comprehensive nano-interpenetrating semiconducting photoresist toward all-photolithography organic electronics, Sci. Adv. 7 (2021) eabg0659.
[49] H. Kweon, K.Y. Choi, H.W. Park, R. Lee, U. Jeong, M.J. Kim, H. Hong, B. Ha, S. Lee, J.Y. Kwon, K.B. Chung, H. Lee, D.H. Kim, Silicone engineered anisotropic lithography for ultrahigh-density OLEDs, Nat. Commun. 13 (2022) 6775.
[50] H.H. Fong, J.K. Lee, Y.F. Lim, A.A. Zakhidov, W.W.H. Wong, A.B. Holmes, C.K. Ober, G.G. Malliaras, Orthogonal processing and patterning enabled by highly fluorinated light-emitting polymers, Adv. Mater. 23 (2011) 735.
[51] L.Z. Qiu, Q. Xu, W.H. Lee, X.H. Wang, B. Kang, G.Q. Lv, K. Cho, Organic thin-film transistors with a photo-patternable semiconducting polymer blend, J. Mater. Chem. 21 (2011) 15637–15642.
[52] T. Park, M. Kim, E.K. Lee, J. Hur, H. Yoo, Overcoming downscaling limitations in organic semiconductors: strategies and progress, Small (2023) 2306468.
[53] C. Kim, K. Kim, O. Kwon, J. Jung, J.K. Park, D.H. Kim, K. Jung, Metal mask material and manufacturing process for high-resolution active-matrix organic light-emitting diode displays, J. Soc. Inf. Disp. 28 (2020) 668–679.
[54] C. Kim, P.E. Burrows, S.R. Forrest, Micropatterning of organic electronic devices by cold-welding, Science 288 (2020) 831–833.
[55] Z. Wang, J. Yuan, J. Zhang, R. Xing, D.H. Yan, Y.C. Han, Metal transfer printing and its application in organic field-effect transistor fabrication, Adv. Mater. 15 (2003) 1009 12.
[56] K. Hoshino, T. Hasegawa, K. Matsumoto, I. Shimoyama, Organic light-emitting diode micro patterned with a silicon convex stamp, Sens. Actuator A Phys. 128 (2006) 339–343.
[57] M. Shtein, P. Peumans, J.B. Benziger, S.R. Forrest, Direct, mask- and solvent-free printing of molecular organic semiconductors, Adv. Mater. 16 (2004) 1615 20.
[58] L. Chen, Y.Z. Hu, H.X. Huang, C. Liu, D. Wu, J.L. Xia, Direct laser patterning of organic semiconductors for high performance OFET-based gas sensors, J. Mater. Chem. C 11 (2023) 7088–7097.
[59] J.M. Chen, D. Li, Y.H. Sun, Y.D. Wang, Z.F. Zeng, L. Jiang, L.F. Chi, Sub-micro organic light emitting diode arrays defined by tip-induced resist hollow structures, Appl. Surf. Sci. 638 (2023) 158033.
[60] G. Kim, D. Kim, Y. Choi, A. Ghorai, G. Park, U. Jeong, New approaches to produce large-area single crystal thin films, Adv. Mater. 35 (2023) 2203373.
[61] M. Gleiche, L.F. Chi, H. Fuchs, Nanoscopic channel lattices with controlled anisotropic wetting, Nature 403 (2000) 173–175.
[62] D.Y. Zhong, K. Wedeking, T. Blomker, T. Erker, H. Fuchs, L.F. Chi, Multilevel supramolecular architectures self-assembled on metal surfaces, ACS nano 4 (2010) 1997–2002.
[63] E. Moulin, J.J. Cid, N. Giuseppone, Advances in supramolecular electronics-from randomly self-assembled nanostructures to addressable self-organized interconnects, Adv. Mater. 25 (2013) 477–487.
[64] L. Wang, Z.Y. Ji, C.Y. Lu, W. Wang, J.W. Guo, L. Li, D.M. Li, M. Liu, Combining bottom-up and top-down segmentation: a way to realize high-performance organic circuit, IEEE Electron Device Lett. 36 (2015) 684–686.
[65] B.Q. Wei, R. Vajtai, Y. Jung, J. Ward, R. Zhang, G. Ramanath, P.M. Ajayan, Organized assembly of carbon nanotubes, Nature 416 (2002) 495–496.
[66] W. Zhang, Z.W. Shi, D.Y. Huo, X.X. Guo, F. Zhang, L.S. Chen, Q.H. Wang, B.S. Zhang, C.S. Peng, In-situ laser nano-patterning for ordered InAs/GaAs (001) quantum dot growth, Appl. Phys. Lett. 112 (2018) 153108.
[67] H.Q. Jia, L.W. Guo, W.X. Wang, H. Chen, Recent progress in GaN-based light-emitting diodes, Adv. Mater. 21 (2009) 4641–4646.
[68] H. Brune, M. Giovannini, K. Bromann, K. Kern, Self-organized growth of nanostructure arrays on strain-relief patterns, Nature 394 (1998) 451–453.
[69] J. Schuster, J. Aberl, L. Vukušić, L. Spindlberger, H. Groiss, T. Fromherz, M. Brehm, F. Schäffler, Photoluminescence enhancement by deterministically site-controlled, vertically stacked SiGe quantum dots, Sci. Rep. 11 (2021) 20597.
[70] A.L. Briseno, S.C.B. Mannsfeld, M.M. Ling, S. Liu, R.J. Tseng, C. Reese, M.E. Roberts, Y. Yang, F. Wudl, Z.N. Bao, Patterning organic single-crystal transistor arrays, Nature 444 (2006) 913–917.
[71] A.L. Briseno, J. Aizenberg, H.Y. Han, R.A. Penkala, H. Moon, A.J. Lovinger, C. Kloc, Z.N. Bao, Patterned growth of large oriented organic semiconductor single crystals on self-assembled monolayer templates, J. Am. Chem. Soc. 127 (2005) 12164–12165.
[72] W. Hu, N. Lu, H. Zhang, Y. Wang, N. Kehagias, V. Reboud, C.M. Sotomayor Torres, J.Y. Hao, W. Li, H. Fuchs, L.F. Chi, Multicolor emission on prepatterned substrates using a single dye species, Adv. Mater. 19 (2007) 2119–2123.
[73] C.Q. Wang, Z.J. Lu, W. Deng, W.Q. Zhao, B. Lu, J. Xiao, X.J. Zhang, J.S. Jie, X.H. Zhang, Precise patterning of single crystal arrays of organic semiconductors by a patterned microchannel dip-coating method for organic field-effect transistors, J. Mater. Chem. C 9 (2021) 5174–5181.
[74] A. Pick, G. Witte, G, Patterned growth of organic semiconductors: selective nucleation of perylene on self-assembled monolayers, Langmuir 32 (2016) 8019–8028.
[75] J. Pan, Y.M. Wu, X.J. Zhang, J.H. Chen, J.W. Wang, S.L. Cheng, X.F. Wu, X.H. Zhang, J.S. Jie, Anisotropic charge trapping in phototransistors unlocks ultrasensitive polarimetry for bionic navigation, Nat. Commun. 13 (2022) 6629.
[76] J.H. Chen, J.W. Wang, S. Chen, J. Pan, R.F. Jia, C.Q. Wang, X.F. Wu, J.S. Jie, X.J. Zhang, Self-limited epitaxial growth of patterned monolayer organic crystals for polarization-sensitive phototransistor with ultrahigh dichroic ratio, Adv. Funct. Mater. 34 (2024) 2308298.
[77] W. Deng, Y. Lv, X.L. Zhang, X.C. Fang, B. Lu, Z.J. Lu, J.S. Jie, High-resolution patterning of organic semiconductor single crystal arrays for high-integration organic field-effect transistors, Mater. Today 40 (2020) 82–90.
[78] W.C. Wang, L.F. Chi, Area-selective growth of functional molecular architectures, Acc. Chem. Res. 45 (2012) 1646–1656.
[79] K. Wedeking, Z.C. Mu, G. Kehr, J. Cano Sierra, C. Mück Lichtenfeld, S. Grimme, G. Erker, R. Fröhlich, L.F. Chi, W.C. Wang, D.Y. Zhong, H. Fuchs, Oligoethylene chains terminated by Ferrocenyl end groups: synthesis, structural properties, cccccand two-dimensional self-assembly on surfaces, Chem. Eur. J. 12 (2006) 1618–1628.
[80] H.Y. Zhang, C. Huo, J.J. Zhang, P. Zhang, W.J. Tian, Y. Wang, Efficient single-layer electroluminescent device based on a bipolar emitting boron-containing material, Chem. Commun. (3) (2006) 281–283.
[81] P.R.L. Malenfant, C.D. Dimitrakopoulos, J.D. Gelorme, L.L. Kosbar, T.O. Graham, A. Curioni, W. Andreoni, N-type organic thin-film transistor with high field-effect mobility based on a N, N'-dialkyl-3,4,9,10-perylene tetracarboxylic diimide derivative, Appl. Phys. Lett. 80 (2002) 2517–2519.
[82] Y.F. Zhao, X.Y. Mu, C.X. Bao, Y. Fan, J.J. Zhang, Y. Wang, Alkyl chain length dependent morphology and emission properties of the organic micromaterials based on fluorinated quinacridone derivatives, Langmuir 25 (2009) 3264–3270.
[83] W.C. Wang, D.Y. Zhong, J. Zhu, F. Kalischewski, R.F. Dou, K. Wedeking, Y. Wang, A. Heuer, H. Fuchs, G. Erker, L.F. Chi, Patterned nucleation control in vacuum deposition of organic molecules, Phys. Rev. Lett. 98 (2007) 225504.
[84] W.C. Wang, C. Du, D.Y. Zhong, M. Hirtz, Y. Wang, N. Lu, L.X. Wu, D. Ebeling, L.Q. Li, H. Fuchs, L.F. Chi, Control over patterning of organic semiconductors: step-edge-induced area-selective growth, Adv. Mater. 21 (2009) 4721–4725.
[85] A.J. Fleming, F.P. Netzer, M.G. Ramsey, Nucleation and 3D growth of para-sexiphenyl nanostructures from an oriented 2D liquid layer investigated by photoemission electron microscopy, J. Condens. Matter Phys. 21 (2009) 445003.
[86] H. Wang, O. Buller, W.C. Wang, A. Heuer, D.Q. Zhang, H. Fuchs, L.F. Chi, Area confined position control of molecular aggregates, New J. Phys. 18 (2016) 053006.
[87] P. Clancy, Application of molecular simulation techniques to the study of factors affecting the thin-film morphology of small-molecule organic semiconductors, Chem. Mater. 23 (2011) 522–543.
[88] O. Buller, H. Wang, W.C. Wang, L.F. Chi, A. Heuer, Boundary-induced nucleation control: a theoretical perspective, Phys. Chem. Chem. Phys. 20 (2018) 3752–3760.
[89] F. Lied, T. Mues, W.C. Wang, L.F. Chi, A. Heuer, Different growth regimes on prepatterned surfaces: consistent evidence from simulations and experiments, J. Chem. Phys. 136 (2012) 024704.

[90] F. Kalischewski, J. Zhu, A. Heuer, Loss of control in pattern-directed nucleation: a theoretical study, Phys. Rev. B 78 (2008) 155401.
[91] Y. Jiang, Y.C. Cai, J.P. Li, N.B. Chen, L.G. Hu, W.C. Wang, Q.M. Nie, B. Yan, Effects of molecular diffusion length on area-selective growth of organic patterns, Mater. Res. Express 9 (2022) 035101.
[92] S.F. Hopp, A. Heuer, Anisotropic behavior of organic molecules on prepatterned surfaces, J. Chem. Phys. 136 (2012) 154106.
[93] W. Tewes, O. Buller, A. Heuer, U. Thiele, S.V. Gurevich, Comparing kinetic Monte Carlo and thin-film modeling of transversal instabilities of ridges on patterned substrates, J. Chem. Phys. 146 (2017) 094704.
[94] Y. Jiang, L. Shi, N.B. Chen, L.G. Hu, W.C. Wang, Q.M. Nie, B. Yan, Area-selective growth for patterning and separation of molecules at allocated sites: designed kinetic Monte Carlo simulation for anisotropic molecules, Results Phys. 44 (2023) 106145.
[95] H. Zhang, G. Liu, W.C. Wang, L.F. Chi, S.L. Yuan, S, Step-edge induced area selective growth: a kinetic Monte Carlo study, RSC Adv. 4 (2014) 25005–25010.
[96] H. Souri, H. Banerjee, A. Jusufi, N. Radacsi, A.A. Stokes, I. Park, M. Sitti, M. Amjadi, Wearable and stretchable strain sensors: materials, sensing mechanisms, and applications, Adv. Intell. Syst. 2 (2020) 2000039.
[97] K.H. Chu, R. Xiao, E.N. Wang, Uni-directional liquid spreading on asymmetric nanostructured surfaces, Nat. mater. 9 (2010) 413–417.
[98] B. Su, Y. Tian, L. Jiang, Bioinspired interfaces with superwettability: from materials to chemistry, J. Am. Chem. Soc. 138 (2016) 1727–1748.
[99] W.C. Wang, C. Du, L.Q. Li, H. Wang, C.G. Wang, Y. Wang, H. Fuchs, L.F. Chi, Addressable organic structure by anisotropic wetting, Adv. Mater. 25 (2013) 2018–2023.
[100] Y. Morikawa, T. Kondo, S. Nagano, T. Seki, Photoinduced 3D ordering and patterning of microphase-separated nanostructure in polystyrene-based block copolymer, Chem. Mater. 19 (2007) 1540–1542.
[101] G.Z. Geng, R.H. Pan, C.S. Li, R.X. Zheng, Y.A. Liu, Z.S. Zhang, C.Z. Gu, J.J. Li, Height-gradiently-tunable nanostructure arrays by grayscale assembly nanofabrication for ultra-realistic imaging, Laser Photonics Rev. 17 (2023) 2300073.
[102] N. Qin, Z.G. Qian, C.Z. Zhou, X.X. Xia, T.H. Tao, 3D electron-beam writing at sub-15 nm resolution using spider silk as a resist, Nat. Commun. 12 (2021) 5133.
[103] T.V. Neumann, M.D. Dickey, Liquid metal direct write and 3D printing: a review, Adv. Mater. Technol. 5 (2020) 2000070.
[104] W.C. Wang, C. Du, C.G. Wang, M. Hirtz, L.Q. Li, J.Y. Hao, Q. Wu, R. Lu, N. Lu, Y. Wang, H. Fuchs, L.F. Chi, High-resolution triple-color patterns based on the liquid behavior of organic molecules, Small 7 (2011) 1403.
[105] H. Wang, W.C. Wang, L.Q. Li, M. Hirtz, C.G. Wang, Y. Wang, Z.Z. Xie, H. Fuchs, L.F. Chi, Tunable organic hetero-patterns via molecule diffusion control, small 10 (2014) 3045–3049.
[106] W.J. Joo, J. Kyoung, M. Esfandyarpour, S.H. Lee, H. Koo, S. Song, Y.N. Kwon, S.H. Song, J.C. Bae, A. Jo, M.J. Kwon, S.H. Han, S.H. Kim, S. Hwang, M.L. Brongersma, Metasurface-driven OLED displays beyond 10,000 pixels per inch, Science 370 (2020) 459–463.
[107] S. Choi, C. Kang, C.W. Byun, H. Cho, B.H. Kwon, J.H. Han, J.H. Yang, J.W. Shin, C.S. Hwang, N.S. Cho, K.M. Lee, H.O. Kim, E. Kim, S. Yoo, H. Lee, Thin-film transistor-driven vertically stacked full-color organic light-emitting diodes for high-resolution active-matrix displays, Nat. Commun. 11 (2020) 2732.
[108] W.C. Wang, C. Du, H. Bi, Y.H. Sun, Y. Wang, C. Mauser, E. Da Como, H. Fuchs, L.F. Chi, Tunable multicolor ordered patterns with two dye molecules, Adv. Mater. 22 (2010) 2764–2769.
[109] X. Yang, Y. Lin, T.Z. Wu, Z.J. Yan, Z. Chen, H.C. Kuo, R. Zhang, An overview on the principle of inkjet printing technique and its application in micro-display for augmented/virtual realities, Opto-Electron. Adv. 5 (2022) 210123.
[110] X.H. Zhang, G.P. Li, S. Mukherjee, W. Huang, D. Zheng, L.W. Feng, Y. Chen, J.L. Wu, V.K. Sangwan, M.C. Hersam, D.M. DeLongchamp, J.S. Yu, A. Facchetti, T.J. Marks, Systematically controlling acceptor fluorination optimizes hierarchical morphology, vertical phase separation, and efficiency in non-fullerene organic solar cells, Adv. Energy Mater. 12 (2022) 2102172.
[111] H. Wang, C.Y. Zhang, J. Zhu, F. Fontein, Y.D. Wang, Y. Wang, H. Fuchs, W.C. Wang, L.F. Chi, Tunable control efficiency of patterned nucleation by post-annealing, J. Mater. Chem. C 5 (2017) 6672–6676.
[112] Z.R. He, J.H. Chen, D.W. Li, Crystal alignment for high performance organic electronics devices, J. Vac. Sci. Technol. A 37 (2019) 040801.
[113] A. Alaei, K. Zong, K. Asawa, T.M. Chou, A.L. Briseño, C.H. Choi, S.S. Lee, Orienting and shaping organic semiconductor single crystals through selective nanoconfinement, Soft Matter 17 (2021) 3603–3608.
[114] M.L. Li, T.C. Jiang, X.G. Wang, H.L. Chen, S. Li, F. Wei, Z.J. Ren, S.K. Yan, X.F. Guo, H.L. Tu, Preparation of highly oriented single crystal arrays of C8-BTBT by epitaxial growth on oriented isotactic polypropylene, J. Mater. Chem. C 8 (2019) 2155–2159.
[115] D. Bharti, V. Raghuwanshi, I. Varun, A.K. Mahato, S.P. Tiwari, Directional solvent vapor annealing for crystal alignment in solution-processed organic semiconductors, ACS Appl. Mater. Interfaces 9 (2017) 26226–26233.
[116] H.B. Wang, F. Zhu, J.L. Yang, Y.H. Geng, D.H. Yan, Weak epitaxy growth affording high-mobility thin films of disk-like organic semiconductors, Adv. Mater. 19 (2007) 2168–2171.
[117] Z.F. Wang, D. Martin-Jimenez, Q.G. Zhong, D. Ebeling, A. Schirmeisen, H. Wang, W.C. Wang, L.F. Chi, Step-edge-induced patterning and orientation control of crystalline organic semiconductor films, Adv. Mater. Interfaces 10 (2023) 2201780.
[118] H. Gau, S. Herminghaus, P. Lenz, R. Lipowsky, Liquid morphologies on structured surfaces: from microchannels to microchips, Science 283 (1999) 46–49.
[119] H. Wang, W.C. Wang, L.Q. Li, J. Zhu, W.C. Wang, D.Q. Zhang, Z.X. Xie, H. Fuchs, Y. Lei, L.F. Chi, Surface microfluidic patterning and transporting organic small molecules, Small 10 (2011) 2549–2552.
[120] H. Wang, S.G. Wang, J.J. Kan, X.Y. Deng, W.C. Wang, M.H. Wu, Y. Lei, Y, Low voltage driven surface micro-flow by Joule heating, RSC adv. 7 (2017) 29464–29468.
[121] X.J. Zhou, Y.C. Cai, M.S. Xu, J.P. Li, C.X. Sheng, Q.Y. Zhang, X.X. Qiu, W.C. Wang, S.S. Xiong, C.X. Cong, Z.J. Qiu, R. Liu, L.G. Hu, Dewetting-assisted patterning of organic semiconductors for micro-OLED arrays with a pixel size of 1 μm, Small Methods 6 (2022) 2101509.
[122] D.L. Tian, Y.L. Song, L. Jiang, Patterning of controllable surface wettability for printing techniques, Chem. Soc. Rev. 42 (2013) 5184–5209.
[123] S.G. Wang, K. Zhang, M.H. Wu, J.M. Chen, L. Jiang, L.Q. Li, L.F. Chi, W.C. Wang, Stamp recyclable contact printing of liquid droplet matrix on various surfaces, J. Mater. Chem. C 5 (2017) 10971–10975.
[124] Q.C. Mu, S.G. Wang, J.P. Li, L.H. Zhou, L.Q. Li, L.F. Chi, W.C. Wang, Multi-species micropatterning of organic materials by liquid droplet array transfer printing, Appl. Phys. Lett. 114 (2019) 183702.
[125] E.J. Miller, Emulsions. Theory and practice, J. Am. Chem. Soc. 80 (1958) 5578–5579.
[126] K. Zhang, X.Y. Deng, Q. Fu, Y. Meng, H.P. Zhao, W.C. Wang, M.H. Wu, Y. Lei, Photolithography-compatible templated patterning of functional organic materials in emulsion, Adv. Sci. 3 (2016) 1500304.
[127] Q.L. Lin, X. Ye, Q. Guo, X.X. Zheng, Q.X. Han, C.C. Li, J.K. Jiang, Y. Liu, X.T. Tao, Homogeneously oriented organic single-crystalline patterns grown by microspacing in-air sublimation, Small Methods 7 (2023) 2201374.
[128] Z.Y. Fang, H. Wang, J.F. Liang, Z.F. Wang, W.C. Wang, F. Huang, Ultrahigh resolution photodetector arrays of organic single microcrystals self-aligned on prepatterned electrodes, Adv. Mater. Technol. 7 (2022) 2101457.
[129] P.F. Sun, D. Liu, F. Zhu, D.H. Yan, An efficient solid-solution crystalline organic light-emitting diode with deep-blue emission, Nat. Photonics 17 (2023) 264–272.
[130] J. Zhu, F. Fontein, H. Wang, Q.G. Zhong, C.L. Li, J.P. Li, B. Wang, L.S. Liao, Y. Wang, L.Z. Huang, H. Fuchs, W.C. Wang, L.F. Chi, Micro organic light-emitting diodes fabricated through area-selective growth, Mater. Chem. Front. 1 (2017) 2606–2612.
[131] J. Zhu, J.P. Li, Q.G. Zhong, H. Wang, L.Z. Huang, F. Fontein, L.G. Hu, R. Liu, H. Fuchs, W.C. Wang, Y.D. Wang, L.F. Chi, Lithography compatible, flexible micro-organic light-emitting diodes by template-directed growth, Small Methods 3 (2019) 1800508.
[132] J.P. Li, Y. Hu, X.H. Liang, J.M. Chen, L.B. Zhong, L.S. Liao, L. Jiang, H. Fuchs, W.C. Wang, Y.D. Wang, L.F. Chi, Micro organic light emitting diode arrays by patterned growth on structured polypyrrole, Adv. Opt. Mater. 8 (2020) 1902105.
[133] H. Wang, H.P. Lin, X. Fan, S. Ostendorp, Y.D. Wang, L.Z. Huang, L. Jiang, Y.Y. Li, G. Wilde, H. Fuchs, W.C. Wang, L.F. Chi, Positioning growth of NPB crystalline nanowires on the PTCDA nanocrystal template, Nanoscale 10 (2018) 10262–10267.
[134] B.B. Fu, F.X. Yang, L.J. Sun, Q. Zhao, D.Y. Ji, Y.J. Sun, X.T. Zhang, W.P. Hu, Challenging bendable organic single crystal and transistor arrays with high mobility and durability toward flexible electronics, Adv. Mater. 34 (2022) 2203330.
[135] H. Wang, F. Fontein, J.P. Li, L.Z. Huang, L. Jiang, H. Fuchs, W.C. Wang, Y.D. Wang, L.F. Chi, Lithographical fabrication of organic single-crystal arrays by area-selective growth and solvent vapor annealing, ACS Appl. Mater. Interfaces 12 (2020) 48854–48860.
[136] X. Yang, L. Ding, Organic semiconductors: commercialization and market, J. Semicond. 42 (2021) 090201.
[137] Y. Huang, E.L. Hsiang, M.Y. Deng, S.T. Wu, Mini-LED, Micro-LED and OLED displays: present status and future perspectives, Light Sci. Appl. 9 (2020) 105.
[138] M. Shibata, Y. Sakai, D. Yokoyama, Advantages and disadvantages of vacuum-deposited and spin-coated amorphous organic semiconductor films for organic light-emitting diodes, J. Mater. Chem. C 3 (2015) 11178–11191.
[139] Y.N. Huang, K.J. Wu, Y.J. Sun, Y.X. Hu, Z.W. Wang, L.Q. Yuan, S.G. Wang, D.Y. Ji, X.T. Zhang, H.L. Dong, Z.M. Gong, Z.Y. Li, X.F. Weng, R. Huang, Y. Cui, X.S. Chen, L.Q. Li, W.P. Hu, Unraveling the crucial role of trace oxygen in organic semiconductors, Nat. Commun. 15 (2024) 626.
[140] F.J. Meyer zu Heringdorf, M.C. Reuter, R.M. Tromp, Growth dynamics of pentacene thin films, Nature 412 (2021) 517–520.
[141] H. Wang, F. Fontein, Y.D. Wang, Z.F. Wang, H. Fuchs, L.Q. Li, W.P. Hu, L.F. Chi, W.C. Wang, In situ observation of organic single micro-crystal fabrication by solvent vapor annealing, J. Mater. Chem. C 9 (2021) 9124–9129.
[142] L.L. Ji, X.P. Wang, Y.Y. Zhang, X.L. Shen, D. Xue, L. Wang, Z. Wang, W.C. Wang, L.Z. Huang, L.F. Chi, In situ and ex situ investigation of the organic-organic interface effect, Acta Phys. -Chim. Sin. 40 (2024) 230400.
[143] X.L. Shen, Y.D. Wang, J.P. Li, Y.K. Chen, Z. Wang, W.C. Wang, L.Z. Huang, L.F. Chi, Performances of pentacene OFETs deposited by arbitrary mounting angle vacuum evaporator, Front. Mater. 7 (2020) 245.
[144] S.D. Quiroga, A. Shehu, C. Albonetti, M. Murgia, P. Stoliar, F. Borgatti, F. Biscarini, A high-vacuum deposition system for in situ and real-time electrical characterization of organic thin-film transistors, Rev. Sci. Instrum. 82 (2011) 025110.
[145] F. Grillo, J. Soethoudt, E.A. Marques, L. de Martín, K. Van Dongen, J.Ruud van Ommen, A. Delabie, Area-selective deposition of ruthenium by area-dependent surface diffusion, Chem. Mater. 32 (2020) 9560–9572.
[146] G. Liu, H. Zhang, G.K. Liu, S.L. Yuan, A kinetic Monte Carlo simulation of organic particles hetero-patterning on template-induced surface, Colloids Surf. A Physicochem. Eng. Asp. 494 (2016) 186–193.
[147] Z.H. Zhang, S.Y. Wang, C.S. Liu, R.Z. Xie, W.D. Hu, P. Zhou, All-in-one two-dimensional retinomorphic hardware device for motion detection and recognition, Nat. Nanotechnol. 17 (2021) 27–32.
[148] I. Stassen, N. Burtch, A. Talin, P. Falcaro, M. Allendorf, R. Ameloot, An updated roadmap for the integration of metal–organic frameworks with electronic devices and chemical sensors, Chem. Soc. Rev. 46 (2017) 3185–3241.

[149] A.P. Ghosh, T.A. Ali, I. Khayrullin, F. Vazan, O.F. Prache, I. Wacyk, Recent advances in small molecule OLED-on-silicon microdisplays, Organic Light Emitting Materials and Devices XIII, Proc. SPIE 7415 (2009) 127–138.
[150] C. Kang, H. Lee, Recent progress of organic light-emitting diode microdisplays for augmented reality/virtual reality applications, J. Inf. Disp. 23 (2022) 19–32.

Wenchong Wang received his PhD degree from the Institute of Physics, Chinese Academy of Sciences, China, in 2003, working on molecular beam epitaxy. He was a research scientist at Madrid Microelectronics Institute, National Centre for Microelectronics, Spain. He is presently a senior research fellow at the Institute of Physics, Münster University, and CeNTech, Germany. His research mainly focuses on the growth of functional materials and their applications in electronics.

Lifeng Chi received her BSc degree in physics and MSc degree in physical chemistry from Jilin University. She earned her PhD degree in 1989 at the Max Planck Institute for Biophysical Chemistry, Goettingen, Germany. She became a professor in physics at the University of Münster in 2004 and was appointed as chair professor at Soochow University in 2012. Her works mainly focus on on-surface reactions, self-assembling on patterned surfaces and the application in electronics.